First-principles computational modelling of novel anti-perovskite halide materials for energy materials applications

Master Thesis
submitted to the Faculty of the
Escola Tècnica d'Enginyeria de Telecomunicació de Barcelona
Universitat Politècnica de Catalunya
by

Pol Benítez Colominas

In partial fulfillment
of the requirements for the master in
ENGINEERING PHYSICS

Advisor: Claudio Cazorla Silva
Co-Advisor: Edgardo Saucedo Silva
Barcelona, May 2023

Contents

List of Figures

List of Tables

List of physical constants

$\hbar$	Planck's constant
c	Speed of light
e	Electron charge
m_e	Electron mass
Z_I	Atomic number of the chemical specie I
M_I	Mass of the chemical specie I
ε_0	Vacuum dielectric constant
k_B	Boltzman's constant

Abstract

Anti-perovskite halides (AH) with formula Ag_3BC (where B=S, Se and C=I, Br, Cl) are a family of semiconductor materials displaying suitable thermal and optoelectronic properties for potential energy material applications, such as photovoltaic and thermoelectric devices. Nevertheless, AH have been little investigated to date, both at the experimental and theoretical levels, hence their stability, structural and vibrational properties remain relatively unknown. In this work, we have studied the representative compound Ag_3SBr with computational first-principles approaches for advancing knowledge in material science and assessing the functional properties of anti-perovskite halides. In particular, we have employed Density Functional Theory (DFT) techniques considering different exchange-correlation functionals and quantum relativistic spin-orbit coupling effects to simulate this material. Our DFT calculations have revealed several interesting results. First, different interesting phases have been found using crystal structure prediction techniques. Second, we have shown that at least four of them are stable phases non previously reported. Among the stable phases a cubic phase with symmetry group $P2_13$ emerges as a very promising candidate structure for the ground state of Ag_3SBr. And third, the computed band gaps approximately range from 1 to 2 eV and the optical absorption coefficients are relatively large ($10^4 - 10^5$ cm^{-1}) over all the whole visible spectrum. Therefore, in view of our theoretical DFT results it can be concluded that (1) new and more detailed experiments are needed to fully characterize AH at the fundamental level, and (2) the optoelectronic and thermodynamic stability properties of Ag_3SBr suggest great potential of AH for photovoltaic applications.

Acknowledgments

I would like to thank Professor Claudi Cazorla for everything he has done for me, the opportunity to work along him, all the help and detailed explanations that he has provided me and specially for all his kindness.

I am grateful with Professor Edgardo Saucedo for giving me the oportunity to collaborate with him and his group and the warm welcome to his group.

I am indebted to Cibrán for all the helpful explanations in my first steps doing DFT simulations and all the interesting conversations that we have maintained.

I am grateful with Ivan for all the explanations about the experimental results and photovoltaic applications, and also with the rest of the members of the photovoltaics group.

I am also grateful with all the GCM members for accepting me in the group and the good vibes in the working place, especially my office colleagues (listed alphabetically): Alejandro, Àlvar, Carlos, Cibrán, Lola, Ming and Wahi.

Lastly, I would also like to thank my friends and my family, especially my parents who always support me and to whom I owe everything I am.

1 Introduction

1.1 Introduction and motivation of this project

Anti-perovskites [1] are inorganic materials with chemical structure A_3BC where B and C are anions and A is a cation, in contraposition with pervoskites [2] having chemical structure ABC_3 where A and B are cations and C is an anion. In Fig. 1 we can visualize these structures.

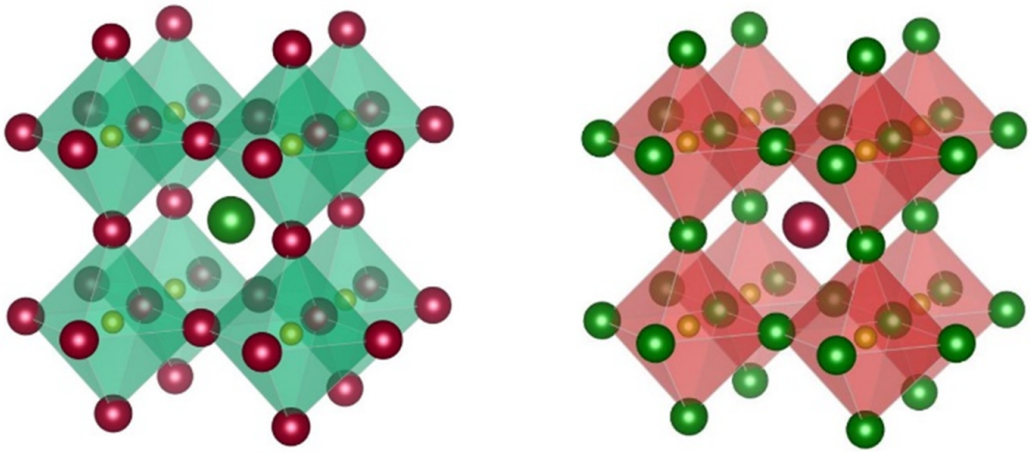

(a) Perovskite (b) Anti-perovskite

Figure 1: Perovskite and anti-perovskite structure comparison. Here green spheres represent cations, while red spheres are anions. It is easy to see that they have the same structure but switching cations and anions places [3].

Despite originally anti-perovskite was used to designate materials with chemical formula A_3BC and the structure shown in Fig. 1b, nowadays it is usual to use anti-perovskite to designate materials with the same composition A_3BC but different structure (as an example one can take a look at Fig. 5, where we can clearly see that almost none of the studied phases of our anti-perovskite material of interest present the structure in Fig. 1b).

Halides refer to the fact that one of the anions of the structure is an halogen atom, then it could be fluoride F^-, chloride Cl^-, bromide Br^-, iodide I^- or astatide As^-. Then for anti-perovskite halides we mean materials with A_3BX where $X=F, Cl, Br, I, As$, while usually $A=Ag$ and $B=S, Se$.

These materials are expected to be great candidates for being used in energy materials applications [3, 4, 5], because their suitable band gaps and optoelectronic properties, and also, of their ion and heat transport properties.

One of the most interesting energy materials applications are photovoltaic applications, as materials for thin film solar cells [6]. A thin film solar layer cell can be thought of a number of thin layers of different materials, where a layer of the desired suitable material can absorb light and uses it to generate electron-hole pairs. With two extra semiconductor layers, we can separate electrons and holes to avoid recombination. Finally, metallic

electrodes can be deposited onto the semiconductor layers in order to extract the photo-generated electrical carriers and create an electrical potential. In Fig. 2 we can see a simplified schematic representation of this device. This is an oversimplified description and in practice a real device will have extra layers and more complex design.

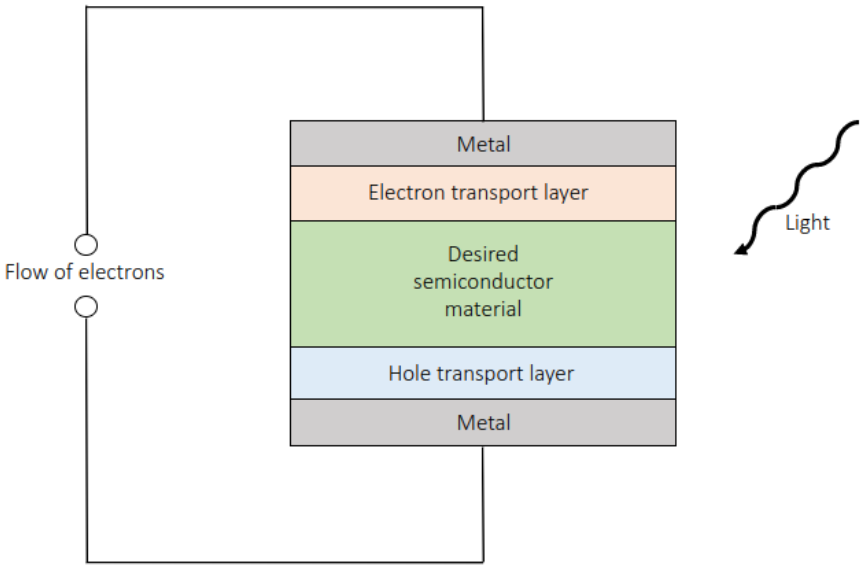

Figure 2: Simplified sketch of a thin film solar cell that generates a flow of electrons as consequence of the absorption of light in the middle layer.

Another interesting application of these materials is as superionic materials [7, 8], since some of they seem to present superionic behaviour [9]. Superionic materials have high ion conductivity, this means that some of the ions can diffuse at ease within the crystalline matrix formed by the other types of atoms. This property can be used, for example, in solid-state batteries and fuel cells.

In this project we will model and characterize Ag_3SBr, an anti-perovskite material that may be useful for some of the explained applications. This material was sintetized and characterized several years ago [9, 10, 11, 12], but a lot of information on its structural and functional properties remain largely unknown. In these papers, different phases were predicted for this material experimentally at different temperatures, but at or near zero temperatures a monoclinic or triclinic phase was observed, and for room temperature a cubic phase with group of symmetries $Pm3m$ [12]. The synthesis and characterization of this material were recently reported in work [13], where a cubic $Pm\bar{3}m$ phase was observed.

1.2 Next chapters overview

This work is organized as follows. In this first chapter, we provide a brief decription of the analyzed materials and the possible applications that they might be suitable for, mainly

photovoltaic applications.

In the following two chapters, we provide a brief description of the computational methods and theory that we have used to model and calculate the properties of a given material.

In the second chapter, we will give a brief introduction of Density Functional Theory (DFT), that is an electronic first-principles method used to numerically solve the quantum Schrödinger equation for the electrons in a condensed matter system. It is a very efficient computational method that allows us to estimate energies, forces and functional properties of materials with a relatively good degree of accuracy.

In the third chapter, we will review basic concepts of Solid State Physics, that we will need to have clear for study the properties of the modelled materials. Remember that Solid State Physics is a theory that uses quantum mechanics and statistical physics formalism to describe the properties of the matter in solid state.

In the fourth chapter, we will provide a brief summary of the procedure that we have followed to find stable structures for our material of interest and then model them to find the different properties. A brief description of the software employed in this project is also provided.

In the fifth chapter, we will present the results of our DFT calculations for the different found phases and the different results obtained for the six final studied phases. Some of the computed values are: energies, phonon dispersion curves, band gaps, optical properties, among others.

Finally, in chapter six and seven, we will provide the conclusions of our work and discuss future research directions on anti-perovskite halide materials.

2 Density Functional Theory

Density Functional Theory (DFT) [14, 15] is a first-principles computational method used to determine the ground-state of many-electron system. DFT is computationally very efficient so that it can be used, for instance, to determine the electronic band structure of solids with reliability. This field has its origin in the work developed by Hohenberg, Kohn and Sham in the 60s [16, 17].

In this section we will give a brief explanation of this method, since we will use it to modellize and simulate our materials of interest.

2.1 The materials many-body problem

Materials are composed of nuclei (or ions) and electrons. The nuclei and electrons in a material, or any other condensed matter system, fundamentally interact through the electrostatic Coulomb interaction.

The time-independent Schrödinger equation of a many-body system is expressed as:

$$\hat{H}\Psi = E\Psi, \tag{2.1}$$

where Ψ is the wave function of the system, $\hat{H}$ is the Hamiltonian operator, and E the energy eigenvalue.

For the particular case of an electron under external potential V, Eq. 2.1 adopts the form:

$$\left(\frac{\mathbf{p}^2}{2m_e} + \hat{V}(\mathbf{r})\right)\Psi = E\Psi, \tag{2.2}$$

where $\hat{V}(\mathbf{r})$ is the external potential that depends on the position of the electron, m_e is the mass of the electron, and $\mathbf{p}$ is the momentum operator that is defined as $\mathbf{p} = -i\hbar\nabla$ ($\hbar$ is Planck's constant, see List of Physical constant in page iv).

To solve the Schrödinger equation of a sytem that contains N electrons and M ions, the corresponding wave function $\Psi(\mathbf{r}_1, \mathbf{r}_2, \ldots, \mathbf{r}_N, \mathbf{R}_1, \mathbf{R}_2, \ldots, \mathbf{R}_M)$ needs to be determined. Note that we have used $\mathbf{r}$ and $\mathbf{R}$ to differentiate between the position of the electrons and the position of the ions, respectively.

The Hamiltonian for this system contains the kinetic and potential energy of the system, and also other external fields:

$$\begin{aligned}\hat{H} = &-\frac{\hbar^2}{2m_e}\sum_i \nabla_i^2 - \sum_{i,I}\frac{Z_I e^2}{|\mathbf{r}_i - \mathbf{R}_I|} + \frac{1}{2}\sum_{i\neq j}\frac{e^2}{|\mathbf{r}_i - \mathbf{r}_j|} \\ &-\sum_I \frac{\hbar^2}{2M_I}\nabla_I^2 + \frac{1}{2}\sum_{I\neq J}\frac{Z_I Z_J e^2}{|\mathbf{R}_I - \mathbf{R}_J|} + \sum_\alpha \hat{H}_\alpha^{\text{external field}}.\end{aligned} \tag{2.3}$$

The first term is the kinetic energy of the electrons, the second is the Coulomb attraction between an electron and an ion, the third term is the Coulomb repulsion between two electrons, the fourth term is the kinetic energy of nuclei, the fifth term is the Coulomb

repulsion between two ions, and the last term contains the different external fields that can be applied to the system (for example, an external electric field).

If we introduce the many particle wave function and this Hamiltonian in Eq. (2.1) we should be able to get the energies of the system, but in practice this equation is very difficult to solve.

To simplify the Hamiltonian presented in Eq. (2.3) we can use the Born-Oppenheimer approximation where we can assume that because the masses of the ions are orders of magnitude larger that the mass of electrons, and then ions are almost static in comparison to the electrons, thus we can get rid of the kinetic part of the ions, $\sum_I \frac{\hbar^2}{2M_I}\nabla_I^2 = 0$.

From here it will be helpful to use Hartree atomic units, $\hbar = m_e = e = \frac{4\pi}{\varepsilon_0} = 1$, just in order to have more readable expressions.

Then we can rewrite the Hamiltonian as:

$$\hat{H} = \hat{T} + \hat{V}_{\text{ext}} + \hat{V}_{\text{int}} + E_{\text{II}} = -\sum_i \frac{1}{2}\nabla_i^2 + \sum_{i,I} V_I\left(|\mathbf{r}_i - \mathbf{R}_I|\right) + \frac{1}{2}\sum_{i\neq j}\frac{1}{|\mathbf{r}_i - \mathbf{r}_j|} + E_{\text{II}}, \quad (2.4)$$

where $\hat{V}_{\text{ext}} = \sum_{i,I} V_I\left(|\mathbf{r}_i - \mathbf{R}_I|\right)$ is the potential that electrons feel because the static ground of ions, $\hat{V}_{\text{int}} = \frac{1}{2}\sum_{i\neq j}\frac{1}{|\mathbf{r}_i - \mathbf{r}_j|}$ is the electron-electron interaction, and E_{II} is the classical interaction between ions and other terms that contribute to the energy of the system but do not affect the distribution of electrons.

Any external potential, as an external electrical field can be included in $\hat{V}_{\text{ext}}$, but we will not include any of them since they are not relevant for our problem, thus from now V_{ext} refers only to the interaction of the electrons with the static ground of ions.

We can also get rid of the term E_{II} since it is just an energy shift and will not be important for the further computations, then $\hat{H} = \hat{T} + \hat{V}_{\text{ext}} + \hat{V}_{\text{int}}$. Note that Hamiltonian defined in Eq. 2.3 (without taking into consideration external fields) can be written as $\hat{H} = \hat{H}_{\text{electrons}} + \hat{H}_{\text{nuclei}}$, and with the Born-Oppenheimer approximation what we do is to consider just the electronic contribution of the Hamiltonian. Thus, from now the wave-function of the system will only depend on the electrons position $\Psi\left(\mathbf{r}_1, \mathbf{r}_2, \ldots, \mathbf{r}_N\right)$.

If we solve Eq. (2.1) using the Hamiltonian Eq. (2.4) we can find the total energy of the system as:

$$E = \frac{\langle\Psi|\hat{H}|\Psi\rangle}{\langle\Psi|\Psi\rangle} = \langle\hat{H}\rangle = \langle\hat{T}\rangle + \langle\hat{V}_{\text{int}}\rangle + \int d^3r V_{\text{ext}}(\mathbf{r})n(\mathbf{r}), \quad (2.5)$$

where $n(\mathbf{r})$ is a central magnitude in DFT, the density of electrons, and will be defined in the next section.

2.2 Hohenberg-Kohn Theorems

From Eq. (2.5) it is appreciated that the energy depend on the many-body wave-function. Thus we can consider the energy of the many-electron quantum system as a functional of the wave-function Ψ:

$$E = \mathcal{F}\left[\Psi\right]. \quad (2.6)$$

A functional is in some sense a generalization of usual functions, where instead of having a map from a set of numbers to another set of numbers, for example $f : \mathbb{R} \to \mathbb{R}$, we instead have a map between a set of functions and a set of numbers, for example $\mathcal{F} : \mathcal{C}^n \to \mathbb{R}$ (where $\mathcal{C}^n$ is the set of continuous functions that have continuous first n derivatives and of course $\mathbb{R}$ is the set of real numbers).

Then Eq. (2.6) tells us that there is a functional $\mathcal{F}$ that relates state Ψ with its energy.

What we will see in this section is that for the ground-state energy is completely determined by the density of electrons of the system n:

$$E_0 = \mathcal{G}\left[n\right], \tag{2.7}$$

i.e., that the ground state of the system can be obtained from n. The density of electrons can be computed as the expected value of the density operator, $\hat{n}(\mathbf{r}) = \sum_{i=1,N} \delta\left(\mathbf{r} - \mathbf{r}_i\right)$:

$$n(\mathbf{r}) = \frac{\langle\Psi|\hat{n}(\mathbf{r})|\Psi\rangle}{\langle\Psi|\Psi\rangle} = N\frac{\int d^3r_2 \ldots d^3r_N \left|\Psi\left(\mathbf{r}, \mathbf{r}_2, \ldots, \mathbf{r}_N\right)\right|^2}{\int d^3r_1 d^3r_2 \ldots d^3r_N \left|\Psi\left(\mathbf{r}_1, \mathbf{r}_2, \ldots, \mathbf{r}_N\right)\right|^2}, \tag{2.8}$$

where N the total number of electrons. If we need we can take into consideration the spin of the electrons in this calculation.

But, we need to announce the theorems that guarantee this, the Hohenberg-Kohn theorems.

Theorem 1 (Hohenberg-Kohn first theorem) *For any system of particles with interaction in an external potential $V_{ext}(\mathbf{r})$, this potential is determined uniquely (except for a constant) by $n_0(\mathbf{r})$, the ground-state particle density.*

Corollary 1.1 *All the properties of the system are completely determined given only $n_0(\mathbf{r})$.*

Theorem 2 (Hohenberg-Kohn second theorem) *It is possible to define a universal functional for the energy in terms of the density of particles, $\mathcal{E}[n]$, valid for any V_{ext}. For a particular V_{ext}, the ground-state energy of the system, E_0, is the global minimum value of this functional, and the density that minimizes the funtcional is $n_0(\mathbf{r})$.*

Corollary 2.1 *The functional $\mathcal{E}[n]$ alone is enough to determine the exact ground-state energy and density.*

The proof of these theorems can be easily found in the bibliography provided in the beginning of the chapter.

These theorems can be schematized with the following diagram:

$$\begin{array}{ccc} V_{\text{ext}}(\mathbf{r}) & \overset{\text{HK}}{\Longleftarrow} & n_0(\mathbf{r}) \\ \Downarrow & & \Uparrow \\ \Psi_i\left(\{\mathbf{r}\}\right) & \Longrightarrow & \Psi_0\left(\{\mathbf{r}\}\right) \end{array} . \tag{2.9}$$

This means that if for a given system of particles we have the external potential $V_{\text{ext}}(\mathbf{r})$, and we solve the Schrödinger equation, Eq. (2.1), we can find the solution states $\Psi_i\left(\{\mathbf{r}\}\right)$,

where one of them will be the ground state $\Psi_0(\{\mathbf{r}\})$. With $\Psi_0(\{\mathbf{r}\})$ one can compute the ground-state density of particles $n_0(\mathbf{r})$ using Eq. (2.8), and finally with Hohenberg-Kohn theorem we are able to obtain again $V_{\text{ext}}(\mathbf{r})$ from $n_0(\mathbf{r})$.

We can use these theorems to re-write Eq. (2.5) with the functional formalism:

$$E_{\text{HK}}[n] = T[n] + E_{\text{int}}[n] + \int d^3r V_{\text{ext}}(\mathbf{r}) n(\mathbf{r}), \tag{2.10}$$

where we use E_{HK} to refer that this energy is computed using the Hohenberg-Kohn theorems. We can define $F_{\text{HK}}[n] = T[n] + E_{\text{int}}[n]$, where we group the functional terms together.

2.3 Kohn-Sham auxiliary system

Kohn and Sham developed an approach to translate the original problem of a many-body interacting particles to an auxiliary problem of many-body non-interacting particles.

For this approach we need to make two assumptions:

1. The exact ground-state density can be represented by the ground-state density of an auxiliary system of non-interacting many-electrons (there is no proof of this for real systems).
2. The auxiliary Hamiltonian contains the usual kinetic operator and an effective local potential $V_{\text{eff}}(\mathbf{r})$ that acts over an electron located in $\mathbf{r}$.

The following diagram schematizes this approach:

$$\begin{array}{ccccccc} V_{\text{ext}}(\mathbf{r}) & \overset{\text{HK}}{\Longleftarrow} & n_0(\mathbf{r}) & \overset{\text{KS}}{\Longleftrightarrow} & n_0(\mathbf{r}) & \overset{\text{HK}_0}{\Longrightarrow} & V_{\text{KS}}(\mathbf{r}) \\ \Downarrow & & \Uparrow & & \Uparrow & & \Downarrow \\ \Psi_i(\{\mathbf{r}\}) & \Longrightarrow & \Psi_0(\{\mathbf{r}\}) & & \psi_{i=1,\ldots,N_e}(\mathbf{r}) & \Longleftarrow & \psi_i(\mathbf{r}) \end{array} . \tag{2.11}$$

Note that the left part of the diagram is just the diagram in Eq. (2.9), but now using the Kohn-Sham approach (KS) we can translate the problem into a new problem that obviously has to verify the Hohenberg-Kohn theorems (here we refer them as HK_0) too. This new problem is a problem of independent particles, thus we can obtain the state $\psi_i(\mathbf{r})$ for each particle in the system.

Because the particles are independent, the wave-function of the system can be expressed with a certain combination (Slater determinant) of wave-functions for each electron ψ_i. Thus the density of electrons can be computed in a easier way with:

$$n(\mathbf{r}) = \sum_i f_i \left|\psi_i(\mathbf{r})\right|^2 . \tag{2.12}$$

Then with the Kohn-Sham approach we can re-write the energy functional obtained for the many-body system through the HK theorems, Eq. (2.10), with the expression:

$$E_{\text{KS}}[n] = T_{\text{s}}[n] + \int d^3r V_{\text{ext}}(\mathbf{r}) n(\mathbf{r}) + E_{\text{Hartree}}[n] + E_{\text{xc}}[n], \tag{2.13}$$

where T_s is the kinetic energy of independent particles:

$$T_s[n] = \frac{1}{2}\sum_{\sigma}\sum_{i=1}^{N^\sigma}\int d^3r\,|\nabla\psi_i^\sigma|^2\,, \tag{2.14}$$

where the summation over σ is to take into account the spin degeneracy, and the summation over i is to take into account the N^σ orbitals of $\psi_i^\sigma(\mathbf{r})$ with the lowest energy ϵ_i^σ; V_{ext} is the external potential due to nuclei and other external fields, E_{Hartree} is given by expression:

$$E_{\text{Hartee}} = \frac{1}{2}\int d^3r d^3r' \frac{n\,(\mathbf{r})\,n\,(\mathbf{r}')}{|\mathbf{r}-\mathbf{r}'|}. \tag{2.15}$$

This term is a mean field approximations where we compute the electron-electron interaction as the interaction of one electron with an effective charge that averages the charge of all the electrons in the system.

Finally, because of the Kohn-Sham approach, we need to add a term E_{xc}, the exchange-correlation energy, that contains all the interactions that we are not aware of and that we have not considered as for example the Pauli exclusion principle (consequence of the statistics of a system of fermions). This term can be expressed as:

$$E_{\text{xc}}[n] = F_{\text{HK}}[n] - (T_s[n] + E_{\text{Hartree}}[n]) \tag{2.16}$$

The problem is that we are not sure of how to compute this term and we should use some approximate expressions. This will be discussed in section 2.5.

Finally, we can try to solve the Kohn-Sham auxiliary equations as a variational problem. After this we will get the Kohn-Sham Schrödinger equations:

$$(H_{\text{KS}}^\sigma - \varepsilon_i^\sigma)\,\psi_i^\sigma(\mathbf{r}) = 0, \tag{2.17}$$

where we can taken into account the spin σ, ε_i are the energy eigenvalues, and H_{KS} is the Kohn-Sham Hamiltonian:

$$H_{\text{KS}}^\sigma(\mathbf{r}) = -\frac{1}{2}\nabla^2 + V_{\text{KS}}(\mathbf{r}), \tag{2.18}$$

with:

$$V_{\text{KS}}(\mathbf{r}) = V_{\text{ext}}(\mathbf{r}) + \frac{\delta E_{\text{Hartree}}}{\delta n(\mathbf{r},\sigma)} + \frac{\delta E_{\text{xc}}}{\delta n(\mathbf{r},\sigma)} = V_{\text{ext}}(\mathbf{r}) + V_{\text{Hartree}}(\mathbf{r}) + V_{\text{xc}}^\sigma(\mathbf{r}). \tag{2.19}$$

2.4 Self-consistent Khon-Sham equations

A practical way of numerically solving the Kohn-Sham equation is through self-consistency. With this method we can approach to the ground-state energy and electronic state of a given system.

The first thing is to start with an initial electron density, $n(\mathbf{r})$ (if we need we can take into account the electron spin, $n^\uparrow(\mathbf{r})$, $n^\downarrow(\mathbf{r})$).

Now we can compute the effective potential:

$$V_{\text{eff}}^{\sigma}(\mathbf{r}) = V_{\text{ext}}(\mathbf{r}) + V_{\text{Hartree}}[n] + V_{\text{xc}}^{\sigma}\left[n^{\uparrow}, n^{\downarrow}\right]. \tag{2.20}$$

Note that the spin is important for the exchange-correlation potential, but not for the Hartree part.

With the KS potential we can compute KS Hamiltonian, and then solve KS equations:

$$\left[-\frac{1}{2}\nabla^2 + V_{\text{eff}^{\sigma}}(\mathbf{r})\right]\psi_i^{\sigma}(\mathbf{r}) = \varepsilon_i^{\sigma}\psi_i^{\sigma}(\mathbf{r}), \tag{2.21}$$

where these equations are just an eigenvalue problem.

Once we have the states for each electron $\psi_i^{\sigma}(\mathbf{r})$ we can recompute the density of electrons with Eq. 2.12, and as now we are taking into account the spin this expression can be rewritten as:

$$n^{\sigma}(\mathbf{r}) = \sum_i f_i^{\sigma}\left|\psi_i^{\sigma}(\mathbf{r})\right|^2. \tag{2.22}$$

And we repeat the process as many times as we want or as many times needed to obtain converged results to a desired level.

For the electrons states, ψ_i, we can take the approach of plane waves where we assume that the state can be expanded as a Fourier Series of plane waves:

$$\psi_i(\mathbf{r}) = \sum_{\mathbf{q}} c_{i,\mathbf{q}} \cdot \frac{1}{\sqrt{\Omega}} \exp\left(i\mathbf{q}\cdot\mathbf{r}\right) = \sum_{\mathbf{q}} c_{i,\mathbf{q}} \cdot |\mathbf{q}\rangle, \tag{2.23}$$

where $c_{i,\mathbf{q}}$ are the expansion coefficients in the basis of orthonormal plane waves $|\mathbf{q}\rangle$, $\mathbf{q}$ are vectors of reciprocal space (see section 3.1), and Ω is the volume of the periodic boundary space, that for crystal will be the unit cell.

This approach is very useful since we know that almost all the periodic functions that appear in physics can be expanded in a Fourier Series, then since our crystal structures are periodic we can use this formalism (see section 3.2.2).

Now it is clear how we can implement this to a computer and get energies, states, forces, stresses, among other physical values, for a desired system.

2.5 Exchange-Correlation functional and Pseudopotentials

In this last section of the DFT chapter we can discuss briefly about the exchange-correlation functional and pseudopotentials, since they are key concepts for Density Functional Theory simulations.

2.5.1 Exchange-Correlation functional

As we have explained, in principle we do not know about the form of $E_{\text{xc}}[n]$, since we use this term to add all the physical interactions that we are not aware of. But we are lucky enough because there are some approaches that are good enough to do practical simulations with correct results.

This term can be expressed as:

$$E_{\text{xc}}[n] = \int d\mathbf{r} n(\mathbf{r}) \epsilon_{\text{xc}}\left([n], \mathbf{r}\right), \tag{2.24}$$

where ϵ_{xc} is the energy per electron at point $\mathbf{r}$ that depends on $n(\mathbf{r}, \sigma)$ near the neighborhood of $\mathbf{r}$, and can be computed with:

$$\epsilon_{\text{xc}}\left([n], \mathbf{r}\right) = \frac{1}{2} \int d^3 r' \frac{\bar{n}_{\text{xc}}\left(\mathbf{r}, \mathbf{r}'\right)}{|\mathbf{r} - \mathbf{r}'|}, \tag{2.25}$$

here $\bar{n}_{\text{xc}}$ is the coupling-constant-averaged hole with expression:

$$\bar{n}_{\text{xc}}\left(\mathbf{r}, \mathbf{r}'\right) = \int_0^1 d\lambda n_{\text{xc}}^{\lambda}\left(\mathbf{r}, \mathbf{r}'\right), \tag{2.26}$$

where finally, $n_{\text{xc}}\left(\mathbf{r}, \mathbf{r}'\right)$ is the exchange-correlation hole around an electron at $\mathbf{r}$, and it can be determined with (without taking into consideration the spin, the expression with the spin can be found in the provided bibliography):

$$n_{\text{xc}}\left(\mathbf{r}, \mathbf{r}'\right) = N(N-1) \int d\mathbf{r}_3 \ldots d\mathbf{r}_N \left|\Psi\left(\mathbf{r}, \mathbf{r}', \mathbf{r}_3, \ldots, \mathbf{r}_N\right)\right|^2. \tag{2.27}$$

There are lots of approaches to approximate $E_{\text{xc}}[n]$, but there are two of them that we are especially interested in because their simplicity and usability, the Local Spin Density Approximation (LSDA or LDA) and the Generalized-Gradient Approximations (GGAs).

In LSDA we consider solids as the limit of an homogeneous gas, then the exchange-correlation energy is computed with:

$$E_{\text{xc}}^{\text{LSDA}}\left[n^{\uparrow}, n^{\downarrow}\right] = \int d^3 r n(\mathbf{r}) \epsilon_{\text{xc}}^{\text{hom}}\left(n^{\uparrow}\left(\mathbf{r}\right), n^{\downarrow}\left(\mathbf{r}\right)\right), \tag{2.28}$$

where ϵ_{xc} is for the homogeneous gas situation.

While GGAs are improved methods that goes further the local approximation and consider the gradient of the denisity:

$$E_{\text{xc}}^{\text{GGA}}\left[n^{\uparrow}, n^{\downarrow}\right] = \int d^3 r n(\mathbf{r}) \epsilon_{\text{xc}}\left(n^{\uparrow}, n^{\downarrow}, \left|\nabla n^{\uparrow}\right|, \left|\nabla n^{\downarrow}\right|, \ldots\right). \tag{2.29}$$

2.5.2 Pseudopotentials

Instead of taking into account all the electrons of the atoms we can work with the ones in the valence band (i.e., those which are involved in chemical bonding) and replace the others by an effective potential, this is the concept of pseudopotential.

This is not necessarily an incorrect approach since the most interior electrons of atoms are strongly bonded with the nuclei and it makes sense to consider all as an effective charge.

It is clear that the election of pseudopotentials is not unique for a given atom since we can take less or more electrons depending on the problem we are facing.

3 Solid State Physics basics

Solid state matter [18, 19] consists of large number of atoms linked between them by different interactions generating a relatively stable structure. The main difference between fluids and solid matter is just the fact that atoms in fluids can move freely, thus the distance between a given particle i and another particle j changes significantly over time in a non-periodic manner. While in solid state, as we have explained, the physical and chemical interactions involved between the atoms restrain the movements of the ions, and at $T = 0$ K we can think of the ions as fixed at equilibrium positions. This is not strictly true when $T > 0$ K, since as we will see in section 3.3 atoms in materials oscillate around their equilibrium positions; however, since these fluctuations in general are small compared to the distance between atoms, such an approximation turns out to be reasonable in many cases.

In solids, ions are arranged according to specific spatial patterns structured in a specific way. Depending on how ions are arranged we can differentiate between amorphous and crystal materials. In an amorphous material the ions are disordered, in contrast with crystal materials where there is a given configuration of ions that it is repeated through space. This last type of solid state materials are easier to study since we can use the periodicity of the structure to simplify our calculations.

The purpose of this section is to remember the basic concepts of crystal materials, and our starting point should be to give a brief mathematical description of crystal periodicity.

3.1 Crystal structures

The basic structural unit of a crystal is the unit cell [20], which upon recursive repetition will generate an infinite periodic structure.

The periodic structure encompasses two elements, a lattice and an atomic basis. A lattice is a set of points in the space such as can be defined as the sum of a set on linearly independent vectors, that are called lattice vectors. In the 3-dimensional case they are usually denoted by $\mathbf{a_1}$, $\mathbf{a_2}$ and $\mathbf{a_3}$, then any point in the lattice is described with a vector $\mathbf{R}$:

$$\mathbf{R} = n_1\mathbf{a_1} + n_2\mathbf{a_2} + n_3\mathbf{a_3}, \tag{3.1}$$

with $n_1, n_2, n_3 \in \mathbb{Z}$. In general, the selection of $\mathbf{a_1}$, $\mathbf{a_2}$ and $\mathbf{a_3}$ is not unique, and different combinations of lattice vectors are valid.

The atomic basis is an atom or atoms that are repeated over the points of the lattice. Then a crystal material can be thought as some atoms of the same or different chemical species repeated over a set of points that compound the lattice. Then we can refer each object in the unit cell with respect the lattice points, the basis.

In 3D there are fourteen lattice types, grouped in seven different crystal structures: cubic, tetragonal, orthorhomic, monoclinic, hexagonal, triclinic and rhombohedral. In addition for each of these groups there are different possible symmetries, i.e., a transformation that maintains the same structure. In total we have 230 different groups of symmetry [21].

Another important concept in the study of crystal solids is the concept of reciprocal space. For a given direct lattice of points $\mathbf{R}$, $\mathbf{G}$ is a point of the reciprocal space if and only if $e^{i\mathbf{G}\cdot\mathbf{R}} = 1$. We can think of the reciprocal lattice as the Fourier transform of the direct lattice.

The reciprocal lattice vectors, $\mathbf{b}$, and the lattice vectors fulfill the relation:

$$\mathbf{a_i} \cdot \mathbf{b_j} = 2\pi\delta_{ij}, \tag{3.2}$$

hence we can write:

$$\begin{cases} \mathbf{b_1} = \frac{2\pi \mathbf{a_2}\times\mathbf{a_3}}{\mathbf{a_1}\cdot(\mathbf{a_2}\times\mathbf{a_3})} \\ \mathbf{b_2} = \frac{2\pi \mathbf{a_3}\times\mathbf{a_1}}{\mathbf{a_1}\cdot(\mathbf{a_2}\times\mathbf{a_3})} \\ \mathbf{b_3} = \frac{2\pi \mathbf{a_1}\times\mathbf{a_2}}{\mathbf{a_1}\cdot(\mathbf{a_2}\times\mathbf{a_3})} \end{cases} . \tag{3.3}$$

The Brillouin zone is the equivalent of the unit cell but in reciprocal space. The first Brillouin zone is the locus of points that are more closer to $\mathbf{G} = 0$ than to any other point of the reciprocal lattice. One easy algorithm to find the Brillouin zones is to draw perpendicular bisector between $\mathbf{G} = 0$ and the rest of reciprocal lattice points $\mathbf{k}$, the area delimited by bisectors that contains $\mathbf{G} = 0$ is the first Brillouin zone.

The reciprocal lattice formalism is very useful because it simplifies our models for crystal solid materials, since we only need to take into account electrons with $\mathbf{k}$ within the first Brillouin zone.

3.2 Electrons in a solid

In this subsection we are interested in describing the behaviour of the electrons in solids [20], and how this helps us to distinguish between conductor materials (metals) and insulators.

3.2.1 Nearly-free electron model

We can start studying the simplest situation where the electrons in our material are free to move, the free electron model. In this model the Hamiltonian is given by the kinetic energy of the electrons $H = \frac{\mathbf{p}^2}{2m_e}$, and we just have to solve Eq. (2.1) using this Hamiltonian. The energy solutions are well known and depend on $\mathbf{k}$:

$$E(\mathbf{k}) = \frac{\hbar^2 |\mathbf{k}|^2}{2m_e}. \tag{3.4}$$

But this model is too simple to encompass the more complex behaviours that are presented in solids as the insulator effect. We can study a model that is slightly more realistic taking into account the potential generated by the ions of the material. Because our materials of interest have crystal structure, the potential created by the ions will be periodic, $V(\mathbf{r}) = V(\mathbf{r}+\mathbf{R})$, with $\mathbf{R}$ a vector of the lattice. Any function that presents the same periodicity that the crystal lattice can be described as a series of plane waves, $e^{i\mathbf{G}\cdot\mathbf{r}}$. Now our Hamiltonian is $H = \frac{\mathbf{p}^2}{2m_e} + V(\mathbf{r})$.

Using perturbation theory we can get a first order solution for this model:

$$E(\mathbf{k}) = E_0(\mathbf{k}) + V_0, \tag{3.5}$$

where V_0 is a constant, and E_0 is the solution of the free electron model, the solution obtained in Eq. (3.4). First order approximation just adds an energy shift in the free electron solution, thus we need to go to higher orders to get more interesting solutions.

At second order, the solution is:

$$E(\mathbf{k}) = E_0(\mathbf{k}) + \sum_{\mathbf{k}'=\mathbf{k}+\mathbf{G};\mathbf{G}\neq 0} \frac{|\langle \mathbf{k}'|V|\mathbf{k}\rangle|^2}{E_0(\mathbf{k}) - E_0(\mathbf{k}')}, \tag{3.6}$$

with:

$$\langle \mathbf{k}'|V|\mathbf{k}\rangle = \frac{1}{L^3}\int \mathbf{dr} e^{i(\mathbf{k}-\mathbf{k}')\cdot\mathbf{r}} V(\mathbf{r}). \tag{3.7}$$

A detailed description of these computations and results is completely out of the scope of this project, and for us will be enough to know that Eq. (3.6) gives us the energies that the electrons can have as a function of their wave vector $\mathbf{k}$.

A different, and more accurate, way of estimating the energy of electrons in a crystal is with first-principles methods like density functional theory, which has been briefly explained in the previous chapter. In this latter case, however, all the electron-electron and electron-ion interactions are explicitly taken into account.

3.2.2 Bloch's Theorem

The Bloch's theorem is presented next without a proof (this can be found, for instance, in [20]), which takes full advantage of the periodicity of crystals and reciprocal space representation.

Theorem 3 (Bloch's theorem) *For an electron in a periodic potential with* $\mathbf{k}$*, its state can be expressed as:*

$$\psi^{\alpha}_{\mathbf{k}}(\mathbf{r}) = e^{i\mathbf{k}\cdot\mathbf{r}} u^{\alpha}_{\mathbf{k}}(\mathbf{r}), \tag{3.8}$$

where the super index α *denotes that we can have degeneration for* $\mathbf{k}$*, and where* $u^{\alpha}_{\mathbf{k}}$ *is periodic in the unit cell and in a way that is possible to take* $\mathbf{k}$ *within the first Brillouin zone.*

3.2.3 Band gap and semiconductor materials

From Eq. (3.6) one can find the energies of the electrons, thus we can study the density of states in the system with a given energy. This density of the states can also be found with the determined energies with DFT calculations and the electron density from Eq. (2.12). We will explain how we can compute this in section 4.2.5.

In the ground state the electrons will fill the less energetic states gradually (remember that electrons are fermions, thus they have to obey the Pauli exclusion principle, this means that electrons can not form Bose-Einstein condensates and that in the ground state

they have to fill excited energy states if the less energetic states are already occupied) without letting empty energy states. The most energetic state occupied is the Fermi level, characterized by E_F.

The main difference between insulator and conductor materials is that a conductor material (or metal) is a material with available states above E_F, then electrons can access that states with a little energy. But for the insulator materials we need the concept of band gap, that is the energy difference between two separated regions of occupied states, the valence and conduction band. Insulator materials have E_F level between these two regions, i.e., energy difference between the highest-energy occupied state (in valence band) and the lowest-energy unoccupied state (in conduction band).

We can visualize this in Fig. 3, where we can clearly see that insulators have their valence band completely full and in order to have electrons in the conduction band they need to get (and a variation of k if the we have indirect band gap).

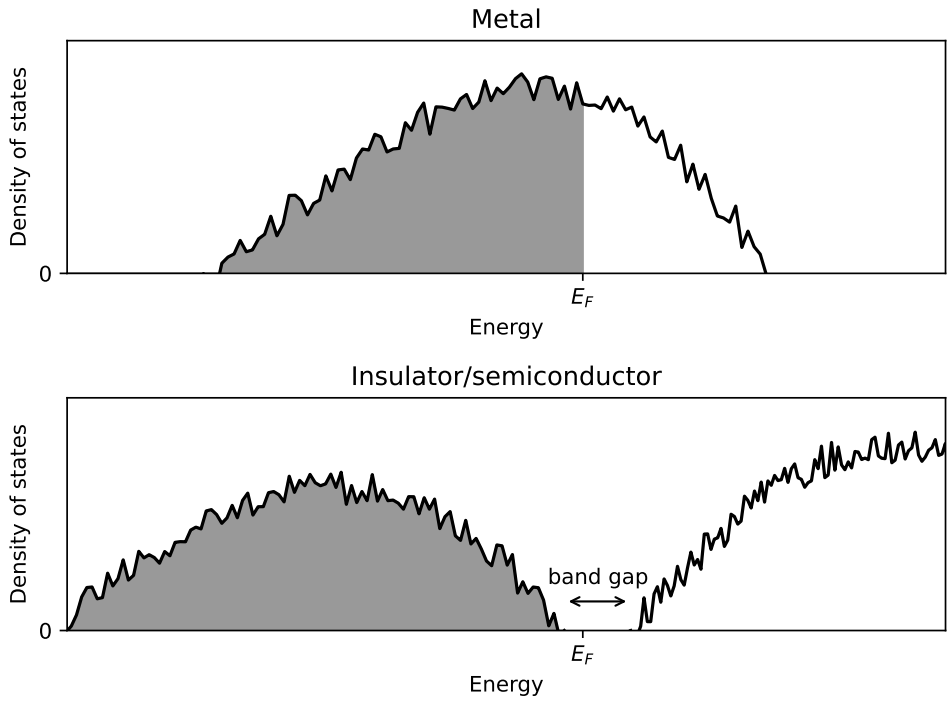

Figure 3: Schematic representation of the density of states occupied by electrons in function of energy for a metal (top) and insulator/semiconductor (bottom) . The grey stripe below the curves represent the occupied states, and E_F is the Fermi level.

Finally, both insulators and semiconductors have the valence band completely fulfilled and the difference is that the band gap for semiconductors is small enough to be sorted under some circumstances (for example, an electron-hole pair can be generated by absorbing a photon (and a phonon with $\mathbf{k}$ for indirect gap) of that energy). Then, semiconductors can behave as conductor materials under these circumstances.

Semiconductor materials [22, 23] present a band gap $E_{\text{gap}} \approx 0.5 - 3.0$ eV. Some classical

examples of semiconductor materials are silicon with $E_{\text{gap}}^{\text{Se}} = 1.1$ eV, [24], or germanium with $E_{\text{gap}}^{\text{Ge}} = 0.67$ eV, [25]. An example of material with bigger band gap and that is considered insulator is diamond with $E_{\text{gap}}^{\text{diamond}} = 5.5$ eV, [26].

We can also distinguish between semiconductors with direct or indirect gap if the minimum of the conduction band and the maximum of the valence band are in the same or in different $\mathbf{k}$, respectively. In direct semiconductors the process of absorbing photons and promote electrons to conduction band does not necessarily involve interacting with phonons, in contrast to indirect semiconductors (due to conservation of the momentum, given by $\mathbf{k}$). On the other hand, once a photo-excited electron-hole pair is created recombination is more difficult to occur in indirect semiconductors (also in this case due to the required involvement of phonons).

3.3 Phonons. Thermal properties

As we explained in the beginning of the section the ions are not necessarily fixed in a given position but they can fluctuate around equilibrium positions at finite temperature. In fact, these ions will move generating oscillations modes with angular frequencies ω, and we can understand these oscillations as particles (or more specifically quasi-particles since they are not really particles but behave as if they were) called phonons [27]. We will see that phonons help us to compute thermodynamic variables of the system.

3.3.1 Lattice vibrations

In order to illustrate the concept of phonons we will provide some explanation for an idealized, non-real, 1D solid, since in this case the solution to the N-body oscillatory problem can be analytically worked out, in contrast to the real 3D case.

In 1D the potential $\phi(x)$ that an ion located in $x = a$ feels can be expanded as a Taylor series:

$$\phi(x) = \phi(a) + \frac{\phi'(a)}{1!}(x-a) + \frac{\phi''(a)}{2!}(x-a)^2 + \dots, \tag{3.9}$$

that in the harmonic approximation we can write it as:

$$\phi(x) \approx \frac{\phi''(a)}{2}(x-a)^2, \tag{3.10}$$

where we have not written $\phi(a)$ since it is a constant that only adds a shift and is no relevant for forces determination. From here one can obtain the force constant $\gamma = \phi''(a)$. The first derivative term vanishes since we are expanding around a minima.

For a single ion the movement under this potential is described by:

$$M\frac{d^2x}{dt^2} = -\gamma x, \tag{3.11}$$

where M is the mass of the ion.

Now if we consider that we have an infinite number of atoms (chain of atoms, since we are in the 1D situation), we will have a system of coupling dynamical equations, one for each atom, for a given atom n the equation is:

$$M\frac{d^2u_n}{dt^2} = -\gamma\left(u_n - u_{n-1}\right) + \gamma\left(u_{n+1} - u_n\right), \tag{3.12}$$

the solution of this system is a set of plane waves with with angular frequency ω, $u_n(t) = ue^{i(kan-\omega t)}$. And the angular frequency depends on k:

$$\omega(k) = 2\sqrt{\frac{\gamma}{M}}\left|\sin\left(\frac{ka}{2}\right)\right|. \tag{3.13}$$

Note that a is the lattice parameter of the unit cell. All the missing steps can be found in the provided bibliography in the beginning of the chapter and in the beginning of the section 3.3.

In Fig. 4 we can see the shape of $\omega(k)$ (bottom curve), it receives the name of acoustic branch because the similarity with sound waves.

Now we can complicate a little bit more this model an add a second specie of atoms in the chain, then for each unit cell we have the two types of atoms. Now the dynamical equations will be more complex:

$$\begin{cases} M_1\frac{d^2u_n}{dt^2} = -\gamma\left(2u_n - v_{n-1} - v_n\right) \\ M_2\frac{d^2v_n}{dt^2} = -\gamma\left(2v_n - u_n - u_{n+1}\right) \end{cases}, \tag{3.14}$$

where u_n denotes atom n of the first chemical specie, and v_n denotes atom n of the second chemical specie.

Again the solution are plane waves, but now $\omega(k)$ can take two values:

$$\omega^2 = \gamma\left(\frac{1}{M_1} + \frac{1}{M_2}\right) \pm \left[\left(\frac{1}{M_1} + \frac{1}{M_2}\right)^2 - \frac{4}{M_1M_2}\sin^2\left(\frac{ka}{2}\right)\right]^{\frac{1}{2}}. \tag{3.15}$$

This means that we have two branches the same acoustic branch that we got for one atom in the unit cell and an optical branch (Fig. 4).

These branches are called phonon dispersion curves, since as we will see a little bit further these oscillations are phonons. The acoustic branches involve in-phase atomic displacements, whereas optical branches involve anti-phase atomic displacements.

Remember that we have assumed an infinite chain of atoms, this is no realistic since real materials contain a finite number of atoms, to solve this we can take as an approximation periodic boundary conditions. As consequence of this restriction k is discretized, $k = \frac{2\pi}{aN}m$, where m is an integer.

Now we can generalize this to the 3D situation with a number n of atoms in the unit cell. The dynamical equations will be very complicated, but we can guarantee that the

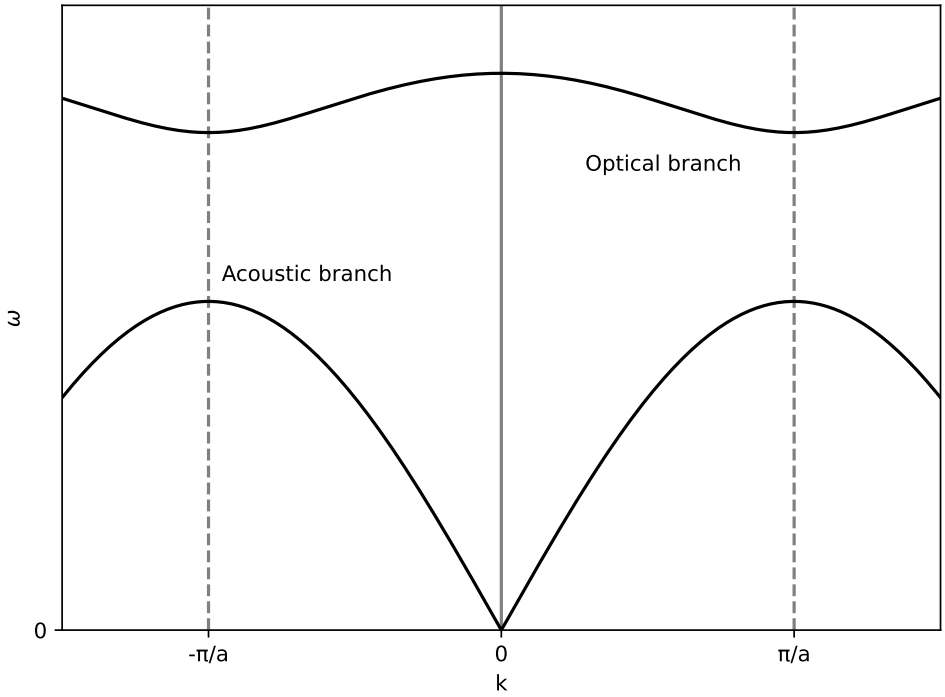

Figure 4: Schematic representation of the acoustic and optical branch for a unit cell with with two different atoms in the first Brillouin zone (delimited by vertical dashed lines) in 1D.

system will have 3 acoustic branches and $3n-3$ optical branches (one for each particle and spatial component). The phonon dispersion curves will be more complex, as a reference we can take a look at Fig. 6. In pure 1D solid only longitudinal modes are possible while in realistic 3D solids transversal modes also exist

3.3.2 Free energy and thermodynamic properties

With phonons we can understand the thermal properties of the material, since one can use statistical physics formalism to find the free energy of the system. In this situation we have a collection of quantum oscillators characterized by their angular frequencies, thus we can compute the free energy of the system [28] with:

$$F = k_B T \sum_n \ln\left(2\sinh\left(\frac{\hbar\omega_n}{2k_B T}\right)\right), \tag{3.16}$$

where the summation is over all the oscillations modes of the material, ω_n.

This computation can be simplified taking into account the first Brillouin zone:

$$F = \frac{k_B T V}{(2\pi)^2}\int_{BZ} d\mathbf{k}\sum_s \ln\left(2\sinh\left(\frac{\hbar\omega_{\mathbf{k},s}}{2k_B T}\right)\right), \tag{3.17}$$

where V is the volume of the first Brillouin zone and s runs over the $3n$ phonon energy levels obtained at every **k**-point.

Once we know the free energy of the system and the energy of the structure that we can determine with DFT, the rest of the thermodynamical variables are easy to compute [29].

3.4 Optical properties

The optical properties of a given material can be computed from the dielectric tensor, $\boldsymbol{\varepsilon}$, with elements ε^{ij} where i denotes the spatial direction of interest while j is the electric current propagation direction, thus in the more general situation one could expect nine different components for this tensor. Despite this, if we assume that the material does not present special spatial directions and therefore it is isotropic, we only need the diagonal elements of ε^{ij}, and all the diagonal elements will have the same value, then we need just one element, ε.

It is important to note that this value will depend on the angular frequency of the light that interacts with the material, $\varepsilon(\omega)$, and in general it is a complex value with real and imaginary part:

$$\varepsilon(\omega) = \varepsilon_1(\omega) + i\varepsilon_2(\omega), \tag{3.18}$$

where it is clear that ε_1 and ε_2 are the real and imaginary part of the dielectric function.

Now from these two real functions it is very easy to compute the different optical properties of the material [30].

The refractive index can be computed with:

$$n(\omega) = \left(\frac{\sqrt{\varepsilon_1^2(\omega) + \varepsilon_2^2(\omega)} + \varepsilon_1}{2} \right)^{\frac{1}{2}}. \tag{3.19}$$

While for the extinction coefficient we can use:

$$\kappa(\omega) = \left(\frac{\sqrt{\varepsilon_1^2(\omega) + \varepsilon_2^2(\omega)} - \varepsilon_1}{2} \right)^{\frac{1}{2}}. \tag{3.20}$$

With $n(\omega)$ and $\kappa(\omega)$ we can determine the reflectivity of the material:

$$R(\omega) = \frac{(n-1)^2 + \kappa^2}{(n+1)^2 + \kappa^2}. \tag{3.21}$$

Finally, the absorption coefficient can be obtained from:

$$\alpha(\omega) = \frac{\sqrt{2}\omega}{c} \left(\sqrt{\varepsilon_1^2(\omega) + \varepsilon_2^2(\omega)} - \varepsilon_1 \right)^{\frac{1}{2}}. \tag{3.22}$$

4 Methodology and simulations

In this chapter, we provide a brief description of the methodology used to find stable phases for the studied material and characterize some of their properties. A little description of some of the software simulation packages is also provided.

4.1 Software used for computational simulations

4.1.1 VASP

VASP (Vienna Ab initio Simulation Package) [31, 32, 33] is a package for doing ab initio simulations of solids, liquids, molecules, surfaces, nanoparticles, among others. It uses DFT methods, but also is possible to use other approaches as many-body perturbation theory.

In order to do a simulation with VASP we need to provide four input files:

1. **POSCAR file**: here is where is specified the lattice geometry and the ions positions.
2. **POTCAR file**: this file contains the pseudopotentials (see section 2.5) values for the atoms that we are interested in simulate.
3. **KPOINTS file**: here we have to specify the **k** points used to sample the first Brillouin zone.
4. **INCAR file**: this is the main file where the parameters and options for the simulation are delcared. There are several number of parameters that we can adjust to produce different types of calculations and with more or less accuracy.

After the simulation the software will output different files depending on what we are computing. For example, if we are doing a relaxation of the crystal structure one of the output files will be a file named CONTCAR with the same information that POSCAR file but with the new ions positions.

Some of the results that we can obtain with VASP simulations and that we have simulated in our project are energies, forces, density of energy states, dielectric tensor, relaxed structures, among others.

4.1.2 Phonopy

Phonopy [34, 35] is an open source software package to do phonon calculations of materials and obtain thermal properties.

As we will see in the next section (section 4.2.3) to obtain the phonon dispersion curves we need to take the structure of interest and produce displacements in the ions, with this displacements we can do DFT simulations and obtain the forces, and with these forces we can obtain the phonon angular frequencies. With Phonopy we can produce this displacements in a easy way and use the symmetry of the phase group, since more symmetric phases need less displacements because some of the forces are equal.

With Phonopy we can also take into account the thermal expansion and do quasi-harmonic computations. The thermal properties are computed using the approach described in section 3.3.2.

4.1.3 VASPKIT

VASPKIT [36] is an open source software to do analysis of raw data obtained from VASP simulations.

With this package we are able to compute many things, some of the utilities that we have used are: obtain the structure, symmetry group and lattice parameters, obtain the ideal path in the reciprocal space for a given structure, produce slightly displacements in the ions of the structure, obtain the optical properties from the dielectric tensor, among others.

4.1.4 VESTA

VESTA [37] is a 3D visualization program that can represent (among other functionalities) the ions positions from the POSCAR file.

The different structure representations in Fig. 5 have been obtained using this software

4.2 Materials modelling

4.2.1 Study of the energy convergence

The first thing we should do before starting with the modelling and characterization of a given material is a study of the convergence of the calculated energy with respect to the number of reciprocal space points and the number of terms that we take in the Fourier Series expansion of the plane wave approach, Eq. (2.23).

If we take more terms in the plane waves expansion or more $\mathbf{k}$ in the reciprocal space the simulation will be more accurate, but the computational time cost will also increase. Since the computation times for these sort of simulations are very high (these simulations can take between minutes and several days in a parallelized computer with hundreds or thousands of CPUs) we have to be sure to take values that give enough accurate results but that are not very time consuming.

A good accuracy in energy for our simulations is around 0.1 meV.

4.2.2 Relaxation of the structure and a first check of stability

Once we have determined the suitable technical parameters for calculating energies and forces explained in section 4.2.1 we are ready to start searching stable phases for the material.

We have to start with a structure for our material, this structure can be one of the expected structures by the experimental results, a structure obtained with structure prediction

software (see section 4.3), or any structure that we consider as possibly energetically competitive.

Now we have to relax this structure, this means that we should determine the atomic arrangement compatible with the imposed symmetry that renders the lowest possible energy. Then we are dealing with a minimization problem. We call this process ionic relaxation. The most usual approach is to use the conjugate-gradient algorithm [38].

We are interested in getting smaller energies because is easy to understand that less energetic phases are more probable than more energetic ones. We can think of it as an $3n$-dimensional space where n is the number of atoms in the unit cell, in this space each point is a possible structure of the material. Then we can map this space to an energy value, $\mathbb{R}^{3n} \to \mathbb{R}$, generating an energy hyper-surface. The minimum of this surface will correspond to meta-stable states (local minimum), while the least energetic state (global minimum) corresponds to the ground-state of the material.

Once the ionic relaxation has finished we can do a first verification of the stability of the resulting structure. For this we can do a phonon determination (see section 4.2.3) in the Γ-point (the center of the Brillouin zone), this is the most symmetric point in the reciprocal space. If as a result we get that there are phonons with imaginary frequencies this means that the structure is not stable. In this situation, we can take the eigenvector of the imaginary phonon mode with higher energy in absolute value and displace the atoms in the unit cell according to its components. With this we are helping the structure to move to a minima in the energy hyper-surface. While if we do not get imaginary frequencies this means that the structure is a good candidate to be stable or meta-stable phase.

We should repeat this process until we get a structure without imaginary frequencies in Γ, and the other points of the reciprocal space.

This ionic relaxation can be done taking into account the structure and group of symmetries or not. In the first case during the ionic relaxation we will maintain the symmetries of the phase and the relaxed material will have the same structure and group of symmetries. While in the second case after an ionic relaxation step the phase structure and symmetries could be different. This second case will be ideal for situations where we are not able to find phases with the desired structure and symmetries (maybe because they do not exist).

4.2.3 Computation of the phonon band dispersion

Once we have a good candidate to stable phase we should compute phonon frequencies for all the points of the reciprocal space.

In order to do this we can compute the dynamical matrix [28, 39] using the results of the DFT simulation:

$$D_{s\alpha,t\beta}(\mathbf{k}) = \frac{1}{\sqrt{M_s M_t}} \sum_l \Phi_{ls\alpha,l't\beta} \exp\left[i\mathbf{k}\cdot(\mathbf{R}_{l'} + \tau_t - \mathbf{R}_s - \tau_s)\right], \tag{4.1}$$

where s refers to the vibration mode, $\mathbf{k}$ is the wave-vector, t is to label the ions, l is for the unit cell, α and β are the Cartesian components, $\Phi_{ls\alpha,l't\beta}$ is the force-constant

matrix (this is what we can get from the DFT simulation), and $\mathbf{R}_{l'} + \tau_t$ is the equilibrium position of atom t in cell l. The vibration frequencies $\omega_{\mathbf{k}s}$ can be found as the eigenvalues of $D_{s\alpha,t\beta}(\mathbf{k})$. For an extensive explanation on how to compute numerically the Eq. (4.1) we refer to [28].

Once we have calculated the phonon frequencies for each point of the reciprocal space, we can represent them by considering a specific reciprocal space path involving the most interesting points in the reciprocal space (high symmetry points), but for different structures and symmetries the shape and the high symmetry points of the reciprocal space are different, then we need a method to determine the optimal path in the **k**-space for each phase. The followed approach is the developed in [40].

Finally, with these phonon frequencies we are able to compute the thermal properties of our studied phase (see section 3.3) using the harmonic approximation. Of course these results will only make sense when the structure does not have imaginary frequencies.

The quasi-harmonic approximation [41] is a correction of the harmonic approximation where we also take into account that the volume of the structure varies with the temperature. By performing DFT phonon calculations at several different volumes, we can apply this correction and obtain more correct Gibbs energies.

4.2.4 Use of different functionals

All the computations done until now should be re-done using other exchange-correlation functionals (see section 2.5).

Remember that we are not sure about the form of the exchange-correlation part, thus there are many different functionals (LSDA or GGAs) such as PBE, PBEsol, SCAN or LDA [42, 43, 44], for each of this potentials the results will be different since they has different expressions, but we expect that if everything is right the results has to be similar. PBE and PBEsol (PBEsol is an improved version of PBE for solids) are generalized-gradient approximation functionals (see section 2.5), these functionals in contrast with LDA consider the gradient of the density. SCAN is a meta-GGA functional since it also includes the second derivative of the electron density.

To use different potentials provide slightly different results for the structural, energy and optoelectronic properties of interest. By comparing to experimental data, or benchmark data obtained with more accurate computational methods, it can decided which functional best describes the system of interest. is a good practices to be sure that everything is going well. Other possibility is compare the results for each functional.

The use of different functionals for the computations explained in sections 4.2.5 and 4.2.6 is also recommended.

4.2.5 Electronic structure and band gap determination

One of the properties of semiconductor materials we are more interested in is the band gap. With it we can be sure that the material is a semiconductor and to know its suitability in energy materials applications.

If we know the density of states (DOS) the band gap can be computed easily (see section 3.2.3) as the difference energy between the last populated states in the valence band and the first in the conduction band. Then, the density of states (DOS), $\bar{n}(\epsilon_i)$ for a pin of energy, can be computed during a DFT simulation of the electronic structure with the expression [45]:

$$\bar{n}(\epsilon_i) = \frac{N(\epsilon_i) - N(\epsilon_{i-1})}{\Delta\epsilon}, \tag{4.2}$$

where ϵ_i is pin of energy of the studied energy range, $\Delta\epsilon$ is the distance between two pins, and where $N(\epsilon_i)$ is the integrated DOS and can be computed with:

$$N(\epsilon_i) = \int_{-\infty}^{\epsilon_i} n(\epsilon_i)\, d\epsilon. \tag{4.3}$$

Finally, the band gap, E_{gap}, can be easily computed with:

$$E_{\text{gap}} = \epsilon_{\text{min}}^{\text{cb}} - \epsilon_{\text{max}}^{\text{vb}}, \tag{4.4}$$

where $\epsilon_{\text{min}}^{\text{cb}}$ and $\epsilon_{\text{max}}^{\text{vb}}$ are respectively the first populated energies of the conduction band and the last of the valence band.

For this type of calculations and for the optical ones (see section 4.2.6) is higly recommended [46, 47] to use hybrid functionals [48] (where the exchange-correlation energy is the exchange-correlation of a GGAs approach plus a Hartree-Fock exchange energy), and take into account the spin-orbit coupling effect (SOC) [49]. The physical reason of this is that we want to minimize electronic self-interaction errors and to take into consideration electronic quantum relativistic effects that become increasingly more important as the radius of the atom increases.

4.2.6 Determination of the optical properties

The last thing we are interested in compute in this work are the optical properties of the materials, again because we are interested in use this materials in optoelectronic applications.

Remember from section 3.4 that to determine the optical properties we just need the dielectric tensor as function of angular frequency or energy.

We can compute this tensor through a DFT simulation using the method explained in [50]. This method tells us that the imaginary part of the tensor (now we will denote the imaginary part by $\varepsilon^{(2)}$ and the real part by $\varepsilon^{(1)}$) can be computed with:

$$\varepsilon_{\alpha\beta}^{(2)}(\omega) = \frac{4\pi^2 e^2}{\Omega} \lim_{q\to 0} \frac{1}{q^2} \sum_{c,v,\mathbf{k}} 2\omega_{\mathbf{k}} \delta(\varepsilon_{c\mathbf{k}} - \varepsilon_{v\mathbf{k}} - \omega) \times \langle u_{c\mathbf{k}+\mathbf{e}_\alpha q} |\, u_{v\mathbf{k}} \rangle \langle u_{v\mathbf{k}} |\, u_{c\mathbf{k}+\mathbf{e}_\beta q} \rangle, \tag{4.5}$$

where α and β are the Cartesian components, c and v refer to conduction and valence band states, $u_{c\mathbf{k}}$ is the cell periodic part of the orbital at $\mathbf{k}$, and Ω is the unit cell volume.

While the real part is computed with:

$$\varepsilon_{\alpha\beta}^{(1)}(\omega) = 1 + \frac{2}{\pi} P \int_0^\infty \frac{\varepsilon_{\alpha\beta}^{(2)}(\omega')\omega'}{\omega'^2 - \omega^2 + i\eta} d\omega', \tag{4.6}$$

where P is used for denote the principle value and η is a complex shift.

4.3 Crystal structure prediction

Crystal prediction of new phases for a given material is a very hard problem [51], since the space of possible phases is huge and the materials simulations are computationally expensive. The crystal structure prediction approaches help us to find possible candidates to be stable phases for a given material, with reasonable computational times. For some materials we may not have an insight of the possible structure that they could have, with this methods is easy to fins some candidates in a fast way.

There are several software packages to find interesting structures, to mention some of them: AIRSS [52], USPEX [53] or CALYPSO [54].

In this work we have used a new approach, MAGUS [55, 56]. This package software uses machine learning methods to find a large amount of possible candidates to be stable phases and check it with VASP calculations, this can be done in few computational time.

To understand well how this method works is out of the scope of this project and the interested reader is encouraged to consult the provided bibliographic references.

5 Results

In this chapter we will explain the different results that we have obtained for the representative anti-perovskite halide compound Ag_3SBr by using computational first-principles methods based on density functional theory.

5.1 Crystal structures

5.1.1 Initial structures: phonons and crystal symmetry breaking

Our first hint at the beginning of our simulations was that the MNT-Solar group at UPC had synthesized and characterized Ag_3SBr and they observed a cubic phase with space group $Pm\bar{3}m$ [13].

Thus we decided to start relaxing a cubic structure with this group of symmetries and with five atoms in the unit cell (three silver atoms, one of bromine, and another one of sulfur). The POSCAR file with the positions for the ions was obtained from Materials Project data set [57]. We were not able to found a stable phase with this structure, thus we allowed for ionic relaxations without maintaining the symmetries.

After several ionic steps we found a triclinic structure with group of symmetry $P1$, that at Γ-point does not present imaginary frequencies. It is important to emphasize that this structures has no symmetries (just the identity) in contrast with the initial cubic that is highly symmetric.

As it is shown in section 5.2, this phase presents some imaginary phonons at some high-symmetry reciprocal space points. Therefore, we constructed a supercell in order to be able to break symmetries by following the eigen-vectors of such imaginary phonons and subsequently relax the structure in the search of a lower energy phase. We found a triclinc phase with symmetries $P1$ and unit cell of fourty atoms is stable at $T = 0$ K. This were good news since an experimental study had previously reported this phase [12].

As this phase contains a large number of atoms in the unit cell and no symmetries at all the computations could take longer than more symmetric phases or with less atoms in unit cell, thus we decided to use FINDSYM software [58] to find very similar phases but with increased symmetry and possibly smaller number of atoms in the unit cell. This package is capable of finding from a given phase other phases with other symmetries. With this we found a trigonal phase with space group $R3$ and twenty atoms in unit cell. After performing several computations we determined that both phases the trigonal and triclinic were the same phase, so we decided to characterize the trigonal since the computations would be faster.

Finally, we decided to study and compute the properties of three of these phases, the cubic $Pm\bar{3}m$ and the triclinic $P1$ (with 5 atoms in the unit cell) because they have been experimentally reported in the literature, and the trigonal $R3$ since it is stable structure.

5.1.2 Adding structures: crystal structure predictions methods

Using MAGUS method for crystal structure prediction [55, 56] we were able to find twenty

new possible stable structures. We computed their energies and studied those with less energy than our trigonal stable phase. The results are presented in the next section 5.1.3.

5.1.3 Structures results

The energies, structures and space groups are showed in this section for the three found phases, the MAGUS obtained phases, and an orthorhombic phase from Materials Project data set that we will use to check if our determined phases could be chemically stable or not.

Symmetry	Space Group	E_0 (eV/f.u.)
Cubic	$P2_13$	-16.905
Orthorhombic	$P2_12_12_1$	-16.826
Cubic	$P2_13$	-16.814
Trigonal	**R3**	**-16.783**
Trigonal	$P3_2$	-16.779
Triclinic	**P1**	**-16.778**
Orthorhombic	$P2_12_12_1$	-16.775
Orthorhombic	$Pna2_1$	-16.765
Orthorhombic*	**Cmcm**	**-16.621**
Cubic	**$Pm\bar{3}m$**	**-16.367**

Table 1: Energies computed with PBEsol functional for the four predicted phases (in bold, and * for the reference phase in material project), and the six less energetic phases found with MAGUS, ordered from less to more energetic.

Symmetry	Space Group	E_0 (eV/f.u.)
Cubic	$P2_13$	-14.832
Orthorhombic	$Pca2_1$	-14.794
Orthorhombic	$P2_12_12_1$	-14.790
Orthorhombic	Pnma	-14.755
Cubic	$P2_13$	-14.753
Monoclinic	$P2_1/c$	-14.747
Trigonal	**R3**	**-14.696**
Triclinic	**P1**	**-14.692**
Orthorhombic*	**Cmcm**	**-14.570**
Cubic	**$Pm\bar{3}m$**	**-14.424**

Table 2: Energies computed with PBE functional for the four predicted phases (in bold, and * for the reference phase in material project), and the six less energetic phases found with MAGUS, ordered from less to more energetic.

In Table 1, 2, 3 and 4 we can find the energies per formula unit (f.u.) and structures computed for each phase (listed from the least energetic to the most energetic) for four different exchange-correlation functionals, PBEsol, PBE, SCAN and LDA respectively.

Symmetry	Space Group	E_0 (eV/f.u.)
Cubic	$P2_13$	-124.229
Orthorhombic	$P2_12_12_1$	-124.139
Cubic	$P2_13$	-124.128
Trigonal	**R3**	**-124.117**
Trigonal	$P3_2$	-124.112
Triclinic	**P1**	**-124.109**
Orthorhombic	$Pna2_1$	-124.106
Tetragonal	$P4_1$	-124.094
Orthorhombic*	**Cmcm**	**-123.977**
Cubic	**$Pm\bar{3}m$**	**-123.831**

Table 3: Energies computed with SCAN functional for the four predicted phases (in bold, and * for the reference phase in material project), and the six less energetic phases found with MAGUS, ordered from less to more energetic.

Symmetry	Space Group	E_0 (eV/f.u.)
Cubic	$P2_13$	-18.803
Orthorhombic	$P2_12_12_1$	-18.736
Cubic	$P2_13$	-18.712
Trigonal	**R3**	**-18.689**
Trigonal	$P3_2$	-18.684
Triclinic	**P1**	**-18.683**
Orthorhombic	$Pna2_1$	-18.666
Monoclinic	$P2_1/c$	-18.653
Orthorhombic*	**Cmcm**	**-18.469**
Cubic	**$Pm\bar{3}m$**	**-18.139**

Table 4: Energies computed with LDA functional for the four predicted phases (in bold, and * for the reference phase in material project), and the six less energetic phases found with MAGUS, ordered from less to more energetic.

We cannot compare the values of energy for a phase obtained with two different functionals, since each functional refers the total energy to a different origin, but we can compare the energy differences between phases provided by them.

For the four functionals the lowest energy phase is a cubic structure with symmetries $P2_13$ that from now we will consider as the ground-state of the Ag_3SBr.

For PBEsol, SCAN and LDA we have computed that there are two more phases with an energy between the energy of the ground-state and the energy of the trigonal $R3$, an orthorhombic phase with space group $P2_12_12_1$ and another cubic $P2_13$. For PBE functional we have obtained three phases between the trigonal and the ground-state, but since these do not appear in the energy ranking obtained with the other three potentials, we disregard them for the subsequent computationally intensive analysis.

Thus, for the subsequent and computationally more intensive calculations, we decided to study these six phases:

- Cubic $P2_13$ (I), the ground-state.
- Orthorhombic $P2_12_12_1$.
- Cubic $P2_13$ (II).
- Trigonal $R3$.
- Triclinic $P1$.
- Cubic $Pm\bar{3}m$.

In Table 5 we can see the number of atoms that these phases have in their unit cell. We can see that the maximum number of atoms in the unit cell is 20, which is not a big number to be able to perform the next simulations.

Phase	# atoms per unit cell
Cubic $P2_13$ (I)	20
Orthorhombic $P2_12_12_1$	20
Cubic $P2_13$ (II)	20
Trigonal R3	20
Triclinic P1	5
Cubic $Pm\bar{3}m$	5

Table 5: Number of atoms per unit cell for each of the six studied phases.

We are interested in determining the formation energy of the ground-state to know if the structure could be chemical stable or not. If this energy is a large positive number the structure will not be chemically stable, but if this energy is negative, or positive with a small value (since in this case temperature effects may end up making the corresponding free energy negative), the structure will be chemically stable.

For this type of calculations, we can use the values provided by Materials Project. For an orthorhombic $Cmcm$ (see Table 1) with determiend energy (with PBEsol) $E = -16.621$ eV the formation energy per atom is $+0.08$ eV. From this we can determine that the ground-state with energy $E = -16.905$ eV should have a formation energy per atom of $+0.023$ eV. This value is small enough to consider that the phase is chemically stable.

In Table 6, 7, 8 and 9 we present the lattice parameters of each phase computed with the functionals PBEsol, PBE, SCAN and LDA, respectively. Comparison with experimental data is not possible here since most of the present phases have not been previously reported in the literature. The obtained results are similar for each exchange-correlation functional, with differences of few 0.1 Å for lattice constants and few degrees for lattice angles.

Phase	a (Å)	b (Å)	c (Å)	α (°)	β (°)	γ (°)
Cubic $P2_13$ (I)	7.586	7.586	7.586	90.000	90.000	90.000
Orthorhombic $P2_12_12_1$	4.518	4.531	21.152	90.000	90.000	90.000
Cubic $P2_13$ (II)	7.584	7.584	7.584	90.000	90.000	90.000
Trigonal R3	8.140	8.140	8.140	109.075	109.075	109.075
Triclinic P1	4.728	4.729	4.727	90.346	90.404	89.580
Cubic $Pm\bar{3}m$	4.793	4.793	4.793	90.000	90.000	90.000

Table 6: Lattice parameters after relaxation with functional PBEsol for each of the six studied phases.

Phase	a (Å)	b (Å)	c (Å)	α (°)	β (°)	γ (°)
Cubic $P2_13$ (I)	7.791	7.791	7.791	90.000	90.000	90.000
Orthorhombic $P2_12_12_1$	4.643	4.649	21.630	90.000	90.000	90.000
Cubic $P2_13$ (II)	7.788	7.788	7.788	90.000	90.000	90.000
Trigonal R3	8.349	8.349	8.349	108.848	108.848	108.848
Triclinic P1	4.860	4.861	4.860	90.958	90.957	89.030
Cubic $Pm\bar{3}m$	4.912	4.912	4.912	90.000	90.000	90.000

Table 7: Lattice parameters after relaxation with functional PBE for each of the six studied phases.

Phase	a (Å)	b (Å)	c (Å)	α (°)	β (°)	γ (°)
Cubic $P2_13$ (I)	7.685	7.685	7.685	90.000	90.000	90.000
Orthorhombic $P2_12_12_1$	4.552	4.612	21.374	90.000	90.000	90.000
Cubic $P2_13$ (II)	7.688	7.688	7.688	90.000	90.000	90.000
Trigonal R3	8.238	8.238	8.238	108.956	108.956	108.956
Triclinic P1	4.803	4.783	4.789	90.380	90.820	89.116
Cubic $Pm\bar{3}m$	4.839	4.839	4.839	90.000	90.000	90.000

Table 8: Lattice parameters after relaxation with functional SCAN for each of the six studied phases.

Phase	a (Å)	b (Å)	c (Å)	α (°)	β (°)	γ (°)
Cubic $P2_13$ (I)	7.478	7.478	7.478	90.000	90.000	90.000
Orthorhombic $P2_12_12_1$	4.454	4.464	20.906	90.000	90.000	90.000
Cubic $P2_13$ (II)	7.476	7.476	7.476	90.000	90.000	90.000
Trigonal R3	8.030	8.030	8.030	109.155	109.155	109.155
Triclinic P1	4.659	4.659	4.660	90.155	90.154	89.832
Cubic $Pm\bar{3}m$	4.728	4.728	4.728	90.000	90.000	90.000

Table 9: Lattice parameters after relaxation with functional LDA for each of the six studied phases.

Finally, in Fig. 5 we can visualize the crystal structure for each phase represented with VESTA.

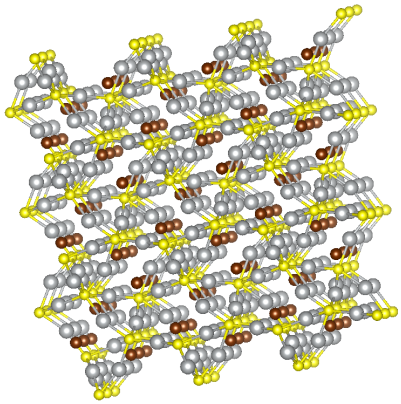

(a) Cubic $P2_13$ (I)

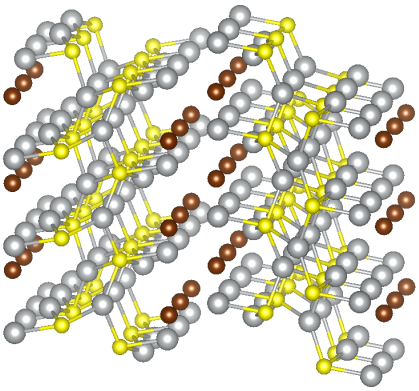

(b) Orthorhombic $P2_12_12_1$

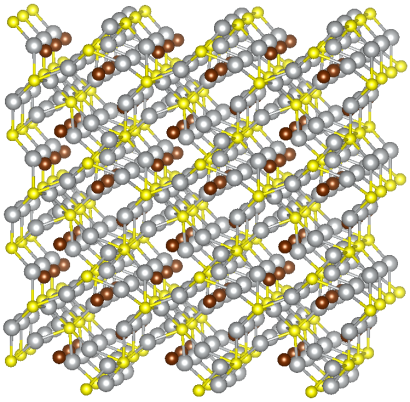

(c) Cubic $P2_13$ (II)

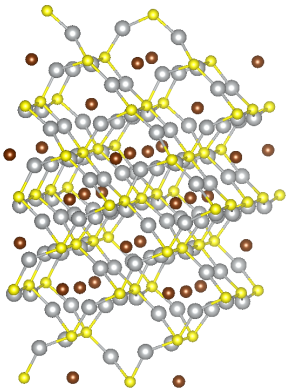

(d) Trigonal R3

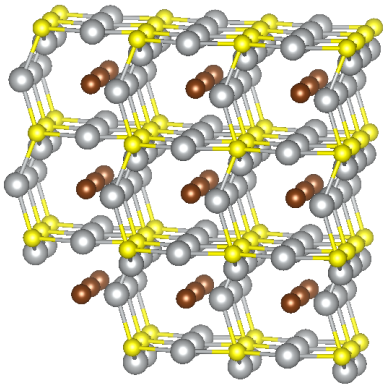

(e) Triclinic P1

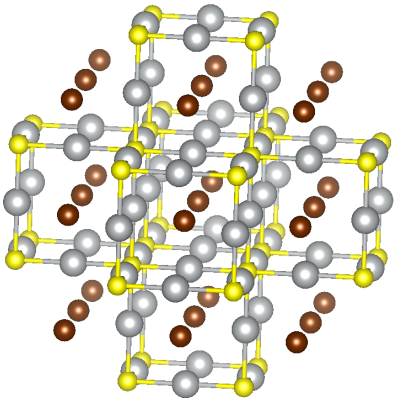

(f) Cubic $Pm\bar{3}m$

(g) Ions legend

Figure 5: Crystal structure of the six studied phases (a-f) represented with VESTA. (g) Legend of which chemical specie represent each color.

5.2 Phonon dispersion curves

In this section, we present the results of computing phonons along specific reciprocal space paths in the first irreducible Brillouin zone for the six phases of interest.

Remember that in order to do these simulations we need to generate a supercell, i.e., replicate the unit cell a certain number of times along each lattice vector direction (in our particular case, 2x2x2), and with VASP and Phonopy we can construct the force constant matrix of your crystal. Then, for each provided **k** point, Phonopy calculates the dynamical force constant matrix and diagonalize it in order to obtain the corresponding eigenfrequencies and eigenmodes.

Once we have determined the eigenfrequencies in each **k**, in order to represent the results we need to select a path in the reciprocal space. The optimal path can be obtained with VASPKIT for a given phase following the approach described in [40].

With this process we can get plots of the phonon frequencies in function of **k**-space points through a path that crosses the most important symmetry points.

In Fig. 6 we can see the results for the six studied phases. The four less energetic phases are stable while the triclinic $P1$ and the cubic $Pm\bar{3}m$ have imaginary frequencies, and thus are not vibrationally stable phases (i.e., correspond to saddle points in the potential energy surface of the material and thus their energies could be lowered by displacing the atoms following the eigenmodes of the imaginary phonon frequencies).

Note that the cubic $Pm\bar{3}m$ has a large amount of imaginary frequencies, this is surprising since it was observed experimentally. One possible argument to justify this is that these calculations at zero-temperature conditions whereas the same phase can be entropically stabilized at finite temperature (see section 7).

Another surprising result is that for the orthorhombic $P2_12_12_1$ phase there is a small pocket of imaginary phonon frequencies around the Γ-point. This suggests that the phase is not really stable, but it could be due to some numerical artifact due to the neglection of multipolar interactions in our DFT simulations [59] (in which only those to second order are exactly taken into account). These corrections would take long times to be computed, thus there is no point in correcting it for this project.

5.3 Competition between the stable phases

With the computed phonon frequencies we can determine the thermodynamic properties of the stable phases (see section 3.3.2), like, for instance, their entropies and free energies.

For each phase we can determine its Gibbs energy using the expression:

$$G_{\text{phase}} = U - TS + pV = E_0^{\text{DFT}} + F^{\text{phonon}}, \tag{5.1}$$

where E_0^{DFT} is the energy determined with DFT simulation, and F^{phonon} is the free energy obtained from phonon frequencies.

For some given p and T conditions, the phase with the lowest Gibbs free will be the stable phase while the others will be meta-stable.

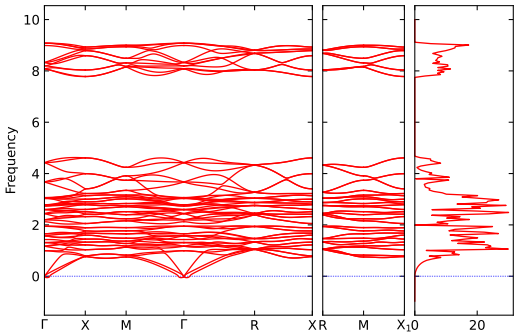

(a) Cubic $P2_13$ (I)

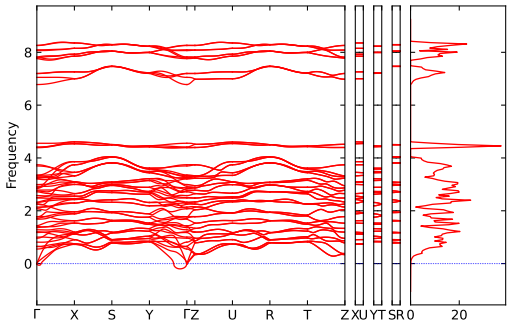

(b) Orthorhombic $P2_12_12_1$

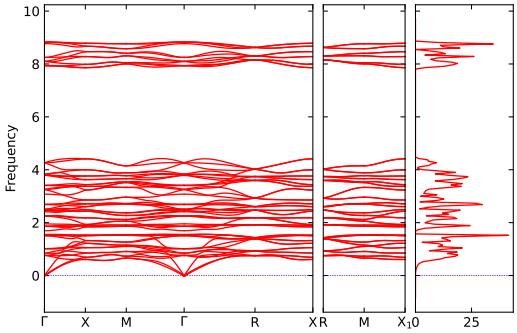

(c) Cubic $P2_13$ (II)

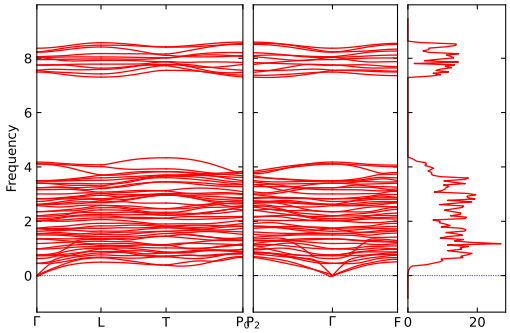

(d) Trigonal R3

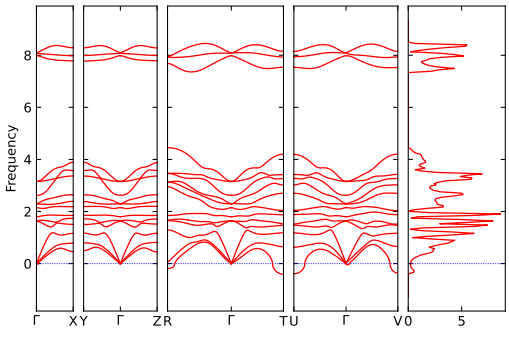

(e) Triclinic P1

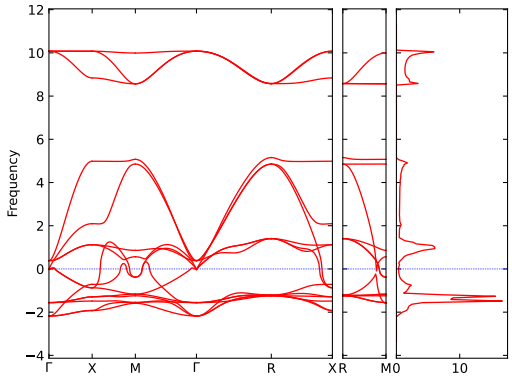

(f) Cubic $Pm\bar{3}m$

Figure 6: Phonon dispersion bands and density of frequencies (THz) computed for each phase (a-f). The first four phases are stable since they do not have phonons with imaginary frequency, while the last two correspond to unstable phases.

5.3.1 Harmonic approximation

The results for the Gibbs energy in function of energy are shown in Fig. 7.

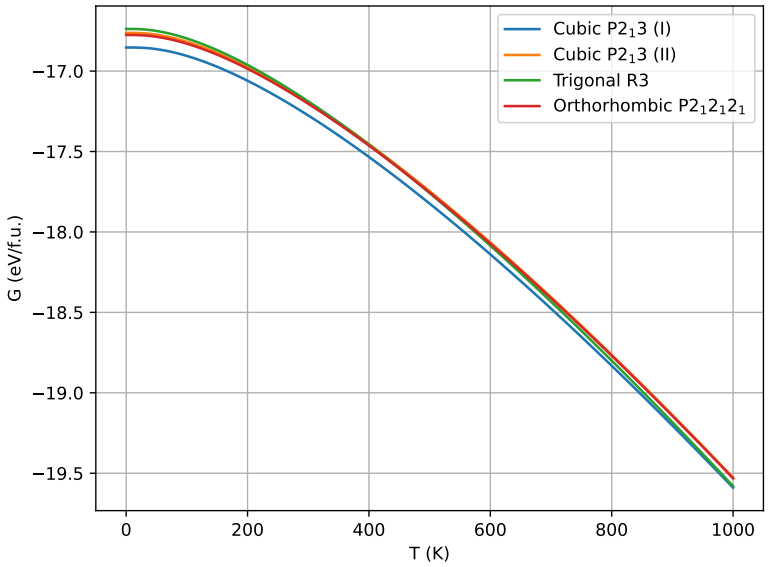

Figure 7: Computed Gibbs Energy per formula unit for the four stable phases in function of temperature. The more favourable phase in this range of temperatures is the cubic P2$_1$3 (I).

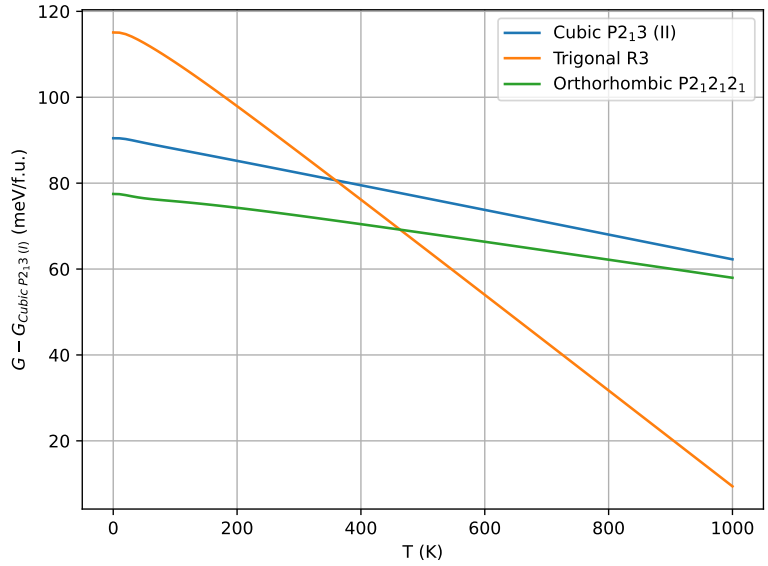

Figure 8: Difference of Gibbs Energy for the three stable phases in relation with the ground state, the cubic P2$_1$3 (I), in function of temperature. For a given temperature a positive value means that the phase is less favourable than the ground state.

We can see that in the range between $T = 0$ K and $T = 1000$ K the phase with the lowest Gibbs free energy is the ground-state, and we cannot expect any phase transition for these temperatures.

In Fig. 8 we have plotted the difference of G between the ground state and the other stables phases. We can see that the most entropic phase (where S is the slope of G) phase is the trigonal. The used exchange-correlation functional for the phonon calculations was PBEsol since it is specially appropriate functional for solid simulations.

5.3.2 Quasi-harmonic approximation

In the quasi-harmonic approximation, we take into account the fact that, for a fixed pressure, the volume of crystal changes with temperature, $V(T)$, hence this provides a more accurate description of phase stability. In adopting this approach, we can reassess the possibility that the trigonal phase becomes the most stable phase at temperatures below 1000 K.

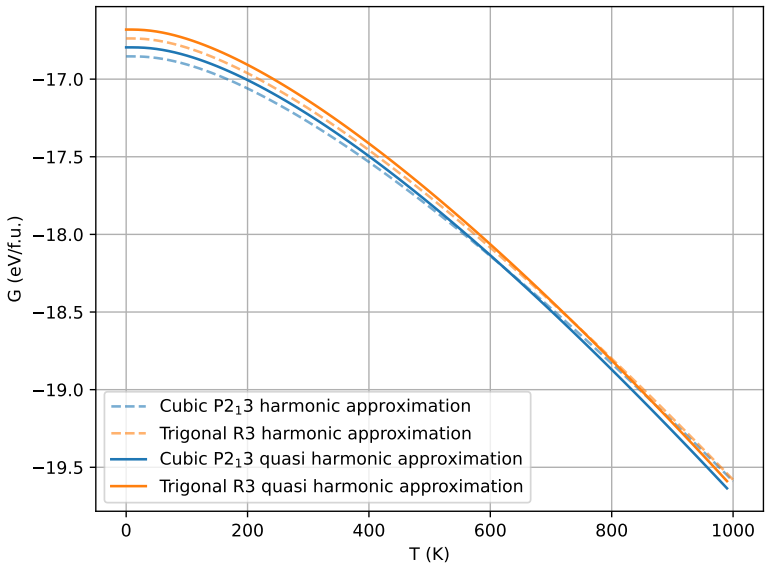

Figure 9: Computed Gibbs Energy per formula unit in function of temperature, for the ground state and the trigonal R3 phase, with the harmonic approximation and using the quasi harmonic approximation correction.

In Fig. 9 we can visualize the results for the ground-state and the trigonal phase in the harmonic and quasi-harmonic approximation. We can see that neither in the quasi-harmonic approximation a phase transition could be expected in the range of temperature between 0 and 1000 K and without pressure.

5.4 Optoelectronic properties

5.4.1 Band gap

In this section, we present the determined band gaps computed following the method described in section 4.2.5.

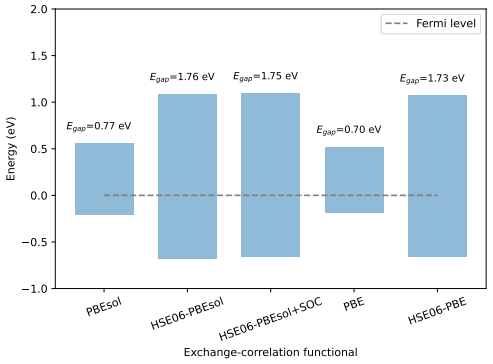

(a) Cubic $P2_13$ (I)

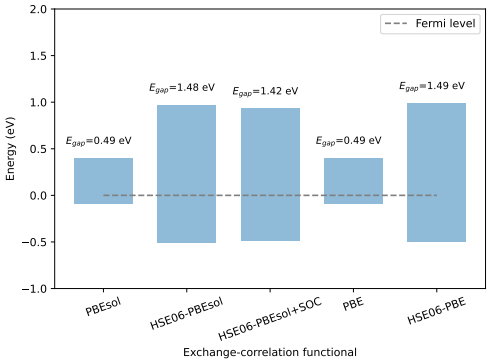

(b) Orthorhombic $P2_12_12_1$

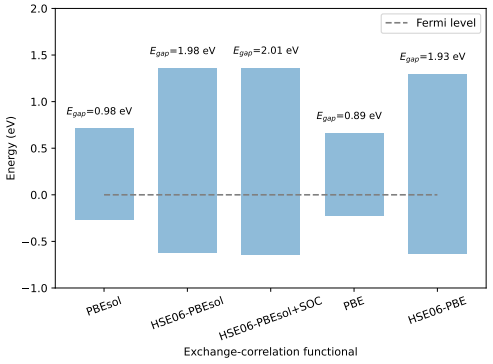

(c) Cubic $P2_13$ (II)

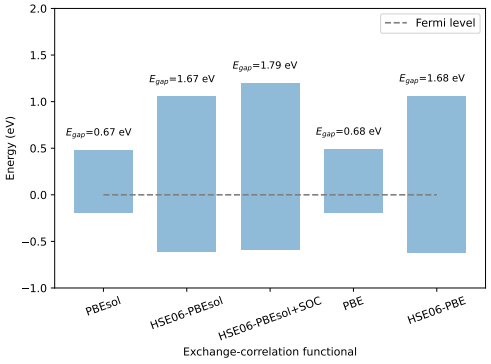

(d) Trigonal R3

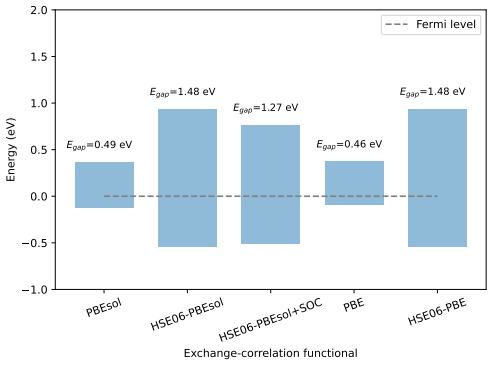

(e) Triclinic P1

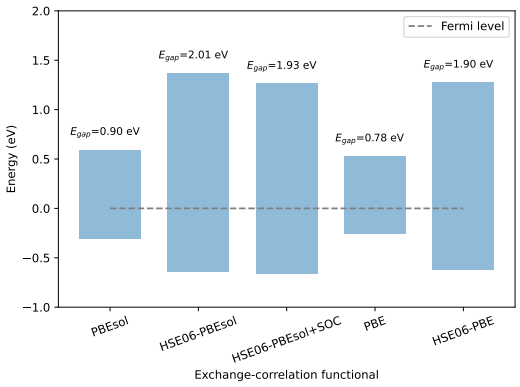

(f) Cubic $Pm\bar{3}m$

Figure 10: Computed band gaps for each of the studied phases (a-f) using different exchange-correlation functionals.

In Fig. 10 we can see the results for each of the phases (also the non-stable ones, because they may be stabilize with temperature) using PBEsol and PBE funtionals, PBEsol and PBE plus Hartree-Fock exchange term (HSE06 hybrid functional), and HSE06-PBEsol with spin-orbit coupling effect (SOC). Remember that without taking into account hybrid functionals and SOC the band gap is usually underestimated.

The importance of using hybrid functionals for these computations is clearly visible, since the band gap value increases significantly, around three times the value obtained without hybrid functionals. We can also see that SOC effect is not very important for our material, it changes the value of the band gap approximately in 0.1 eV.

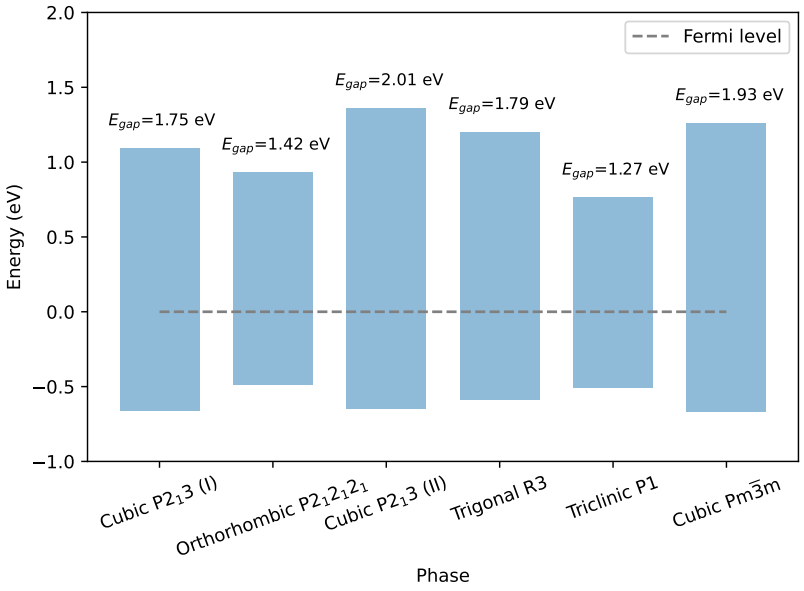

Figure 11: Computed band gaps for each phase with the functional HSE06-PBEsol and taking into account the spin-orbit coupling.

In Fig. 11 we can see the band gaps computed for each phase with the most precise functional, HSE06-PBEsol plus SOC. The expected band gaps range from 1.27 eV to 2.01 eV, then all the phases are semiconductor materials with a suitable band gap for optoelectronic applications since the band gap values are within the interval of visible light frequencies.

5.4.2 Optical properties

Here we show the results for the optical properties determined with the expressions from section 3.4 using the dielectric tensor determined with the explained approach in section 4.2.6.

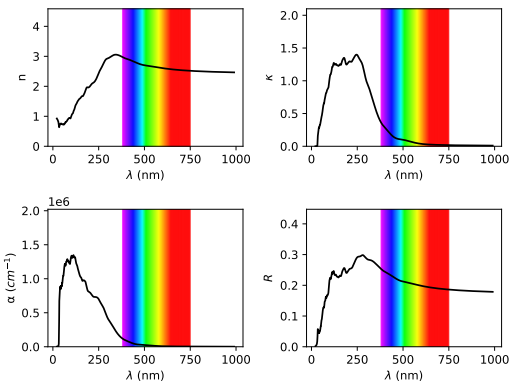

(a) Cubic $P2_13$ (I)

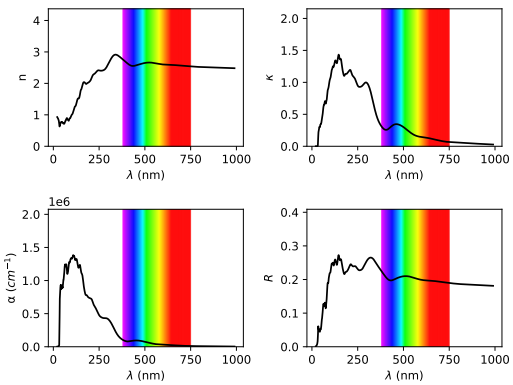

(b) Orthorhombic $P2_12_12_1$

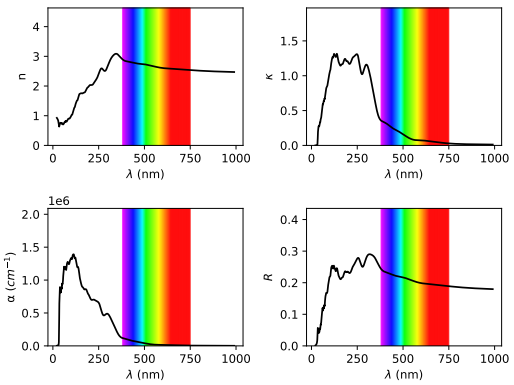

(c) Cubic $P2_13$ (II)

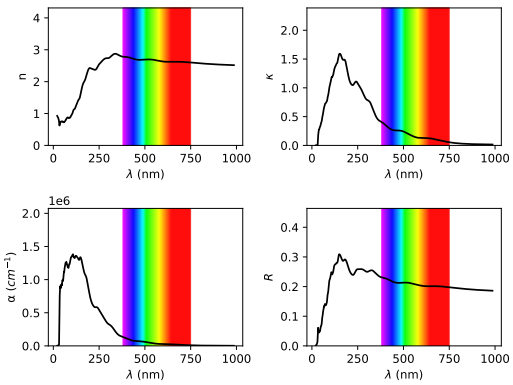

(d) Trigonal R3

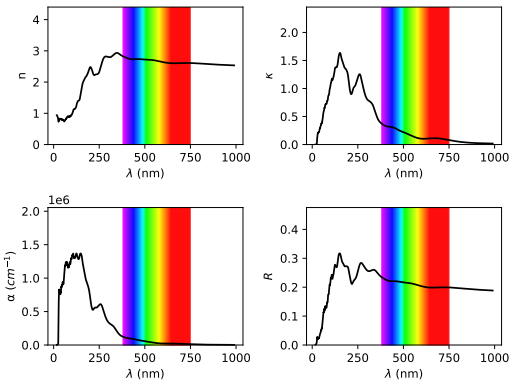

(e) Triclinic P1

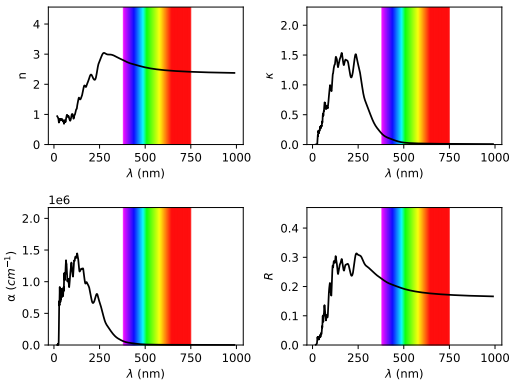

(f) Cubic $Pm\bar{3}m$

Figure 12: Optical properties computed in function of the wavelength for each of the six studied phases (a-f). The four optical properties computed are the refractive index n, the extinction coefficient κ, the absorption coefficient α, and the reflectivity R. The rainbow stripe indicates the visible light spectrum.

In Fig. 12 we can see the obtained refractive index, extinction coefficient, absorption

coefficient and reflectivity, in function of the wave-length for the six phases. The results are similar for all the phases, n and R are small for high energetic light and almost constant for long wave-lengths, while κ and α have high values for high energetic light and decrease fast for longer wave-lengths.

For all the phases n takes a maximum value of approximately 3 for ultraviolet wavelengths. For the extinction coefficient the maximum value is around 1.5 in the same region that the maximum of n. For R the maximum value is around 0.4.

For optoelectronic applications, such as photovoltaic cells we are specially interested in the results obtained for the absorption coefficient. In Fig. 13 we have represented this coefficient for each phase. We can see that the best absorber (the one with highest absorption values) is the orthorhombic phase, and that the ground-state is a better absorber for higher energies. Despite this, all the phases seem to be good absorbers for almost all the visible spectrum. For all the phases the absorption coefficient takes values between 10^3 and 10^5 in the visible spectrum. The worst absorber is the cubic $Pm\bar{3}m$, the best absorber for low energies are the $P2_12_12_1$, $P1$ and $R3$, while for high energies all the phases (except for the $Pm\bar{3}m$ phase) present similar results.

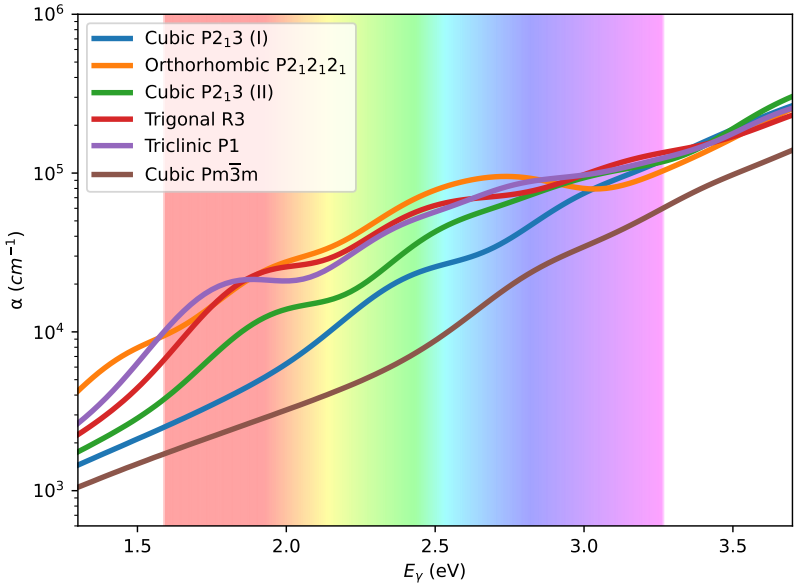

Figure 13: Absorption coefficient in logarithmic scale in function of photon energy for each of the six studied phases. The rainbow stripe indicates the visible light spectrum.

6 Conclusions

We have found a series of stable and metastable phases for the archetypal antiperovskite halide compound AgSBr, which have not been reported previously in experimental nor theoretical studies. One of them stands out as it seems to be the true ground-state of the material, a cubic phase with symmetry group $P2_13$ and twenty atoms per unit cell. Despite that at zero-temperature conditions there are other energetically competitive phases (orthorhombic $P2_12_12_1$, another cubic $P2_13$ and a trigonal $R3$), we have proved that there is no phase transition at least below temperatures of 1000 K, from the results obtained with the harmonic and the quasi-harmonic approximation.

We have not been able to confirm the stability of the $Pm\bar{3}m$ phase as determined by experimentalists, because the zero-temperature energy of this phase lies approximately 0.1 meV/f.u. above that of the lowest energy phase found in our DFT simulations, and the computed zero-temperature phonon spectrum exhibits imaginary phonon branches, thus frustrating the estimation of the Gibbs free energy for this phase. Possible reasons for this lack of agreement can be that either the experimental measurements were over a slightly different chemical compound or that this phase might stabilize with temperature. In any case, the electronic energy at $T = 0$ K for this phase computed with Density Functional Theory techniques is large higher than the energy for the new ground-state and it is not very clear that with anharmonic corrections we could solve this problem.

We have observed that PBEsol, SCAN and LDA exchange-correlation functionals provide similar energetic results. The PBE exchange-correlation functional, however, for some of the phases (appears a $Pca2_1$ phase above the $P2_12_12_1$, the second $P2_13$, and the $R3$, while this does not happen for the other functionals) become more or less energetic than others. We also have been able to observe that hybrid functionals provide significantly different results (and more accurate) than standard GGA and meta-GGA functionals, and that the spin-orbit coupling is not so important for our material.

Finally, we have obtained very interesting optoelectronic properties for the different studied phases, and it seems that this material could be a good candidate for photovoltaic applications. The band gap values are good enough (ranging between $1.5 - 2.0$ eV) to have a material that can absorb light in all the visible spectrum and the obtained absorption coefficients are high enough (up to 10^5 cm^{-1} for all the phases) to be used as a semiconductor material for single-junction solar cells or tandem devices.

7 Further work

Some of the next steps in this work are very clear. First, by using anharmonic phonon approaches, we can compute the temperature-renormalized phonon spectrum of all the investigated phases, thus getting rid of the zero-temperature constrain in our analysis. This can be done using some specific software packages that helps us with this simulations as hiPhive package [60], or DynaPhoPy package [61]. With this computations we should be able to obtain more exact Gibbs energies and see if some vibrationally unstable materials at $T = 0$ K conditions may become entropically stabilized at finite temperature conditions.

It also would be interesting to measure another properties of the material such as energy band diagram, that will give information about if the material has direct or indirect band gap. Other properties of interest are the thermal conductivity, anharmonicity and ion transport. And because the main applications are expected to be in photovoltaics, it would be interesting to study the formation energy of point defects since these can act as non-radiative recombination centers for photo-excited electron-hole pairs.

Of course, one of the most interesting options is to repeat these simulations for the other materials of this family Ag_3BC with B=S, Se and C=I, Br, Cl.

Finally, other possibilities would be to do some basic device simulations in order to verify the suitability of anti-perovskite halides for real devices and their optimization in tandem solar cells.

References

[1] Sergey V Krivovichev. Minerals with antiperovskite structure: a review. *Zeitschrift für Kristallographie-Crystalline Materials*, 223(1-2):109–113, 2008.

[2] AS Bhalla, Ruyan Guo, and Rustum Roy. The perovskite structure—a review of its role in ceramic science and technology. *Materials research innovations*, 4(1):3–26, 2000.

[3] Francisco Palazon. Metal Chalcohalides: Next Generation Photovoltaic Materials? *Solar RRL*, 6(2):2100829, 2022.

[4] Zhiyang Liu, Ruixiang Mi, Guoqi Ji, Yingmeng Liu, Pengfei Fu, Sanlue Hu, Bing Xia, and Zewen Xiao. Bandgap engineering and thermodynamic stability of oxyhalide and chalcohalide antiperovskites. *Ceramics International*, 47(23):32634–32640, 2021.

[5] Uma V Ghorpade, Mahesh P Suryawanshi, Martin A Green, Tom Wu, Xiaojing Hao, and Kevin M Ryan. Emerging Chalcohalide Materials for Energy Applications. *Chemical Reviews*, 2022.

[6] KL Chopra, PD Paulson, and V Dutta. Thin-film solar cells: an overview. *Progress in Photovoltaics: Research and applications*, 12(2-3):69–92, 2004.

[7] RC Agrawal and RK Gupta. Superionic solid: composite electrolyte phase–an overview. *Journal of materials science*, 34(6):1131–1162, 1999.

[8] Malcolm D Ingram. Superionic glasses: theories and applications. *Current Opinion in Solid State and Materials Science*, 2(4):399–404, 1997.

[9] Takashi Sakuma and Sadao Hoshino. The phase transition and the structures of superionic conductor Ag_3SBr. *Journal of the Physical Society of Japan*, 49(2):678–683, 1980.

[10] T Takahashi and O Yamamoto. The $Ag/Ag_3SI/I_2$ solid-electrolyte cell. *Electrochimica Acta*, 11(7):779–789, 1966.

[11] S Hoshino, H Fujishita, M Takashige, and T Sakuma. Phase transition of Ag_3SX (X= I, Br). *Solid State Ionics*, 3:35–39, 1981.

[12] Hiroyuki Honda, Khairul Basar, Sainer Siagian, Takashi Sakuma, Haruyuki Takahashi, Hitoshi Kawaji, and Tooru Atake. Low-Temperature Phase in Superionic Conductor $Ag_3SBr_xI_{1-x}$. *Journal of the Physical Society of Japan*, 76(11):114603, 2007.

[13] Ivan Caño, Jonathan Turnley, Alejandro Navarro, José Miguel Asensi, Rakesh Agrawal, and Edgardo Saucedo. Synthesis of Ag_3SX (X = Br, I) chalcohalide antiperovskite thin films (to be sumbitted).

[14] Richard M Martin. *Electronic structure: basic theory and practical methods*. Cambridge university press, 2020.

[15] Feliciano Giustino. *Materials modelling using density functional theory: properties and predictions*. Oxford University Press, 2014.

[16] Pierre Hohenberg and Walter Kohn. Inhomogeneous electron gas. *Physical review*, 136(3B):B864, 1964.

[17] Walter Kohn and Lu Jeu Sham. Self-consistent equations including exchange and correlation effects. *Physical review*, 140(4A):A1133, 1965.

[18] Neil W Ashcroft and N David Mermin. *Solid state physics*. Cengage Learning, 2022.

[19] Charles Kittel. *Introduction to solid state physics*. John Wiley & sons, inc, 2005.

[20] Steven H Simon. *The Oxford solid state basics*. OUP Oxford, 2013.

[21] Mois Ilia Aroyo, Juan Manuel Perez-Mato, Cesar Capillas, Eli Kroumova, Svetoslav Ivantchev, Gotzon Madariaga, Asen Kirov, and Hans Wondratschek. Bilbao Crystallographic Server: I. Databases and crystallographic computing programs. *Zeitschrift für Kristallographie-Crystalline Materials*, 221(1):15–27, 2006.

[22] Simon Min Sze. *Semiconductor devices: physics and technology*. John wiley & sons, 2008.

[23] Lev I Berger. *Semiconductor materials*. CRC press, 1996.

[24] W Bludau, A Onton, and W Heinke. Temperature dependence of the band gap of silicon. *Journal of Applied Physics*, 45(4):1846–1848, 1974.

[25] Peter J Collings. Simple measurement of the band gap in silicon and germanium. *American Journal of Physics*, 48(3):197–199, 1980.

[26] JT Glass, R Messier, and Naoji Fujimori. Diamond, silicon carbide and related wide bandgap semiconductors. Technical report, Pittsburgh, PA (USA); Materials Research Society, 1990.

[27] Philip Hofmann. *Solid state physics: an introduction*. John Wiley & Sons, 2022.

[28] Dario Alfè. PHON: A program to calculate phonons using the small displacement method. *Computer Physics Communications*, 180(12):2622–2633, 2009.

[29] Raj Kumar Pathria. *Statistical mechanics*. Elsevier, 2016.

[30] Mark Fox. Optical properties of solids, 2002.

[31] Georg Kresse and Jürgen Hafner. Ab initio molecular-dynamics simulation of the liquid-metal–amorphous-semiconductor transition in germanium. *Physical Review B*, 49(20):14251, 1994.

[32] Georg Kresse and Jürgen Furthmüller. Efficiency of ab-initio total energy calculations for metals and semiconductors using a plane-wave basis set. *Computational materials science*, 6(1):15–50, 1996.

[33] Georg Kresse and Jürgen Furthmüller. Efficient iterative schemes for ab initio total-energy calculations using a plane-wave basis set. *Physical review B*, 54(16):11169, 1996.

[34] Atsushi Togo and Isao Tanaka. First principles phonon calculations in materials science. *Scripta Materialia*, 108:1–5, 2015.

[35] Atsushi Togo. First-principles Phonon Calculations with Phonopy and Phono3py. *Journal of the Physical Society of Japan*, 92(1):012001, 2023.

[36] Vei Wang, Nan Xu, Jin-Cheng Liu, Gang Tang, and Wen-Tong Geng. VASPKIT: A user-friendly interface facilitating high-throughput computing and analysis using VASP code. *Computer Physics Communications*, 267:108033, 2021.

[37] Koichi Momma and Fujio Izumi. VESTA 3 for three-dimensional visualization of crystal, volumetric and morphology data. *Journal of applied crystallography*, 44(6):1272–1276, 2011.

[38] William H Press, Saul A Teukolsky, William T Vetterling, and Brian P Flannery. *Numerical recipes 3rd edition: The art of scientific computing*. Cambridge university press, 2007.

[39] Laurent Chaput, Atsushi Togo, Isao Tanaka, and Gilles Hug. Phonon-phonon interactions in transition metals. *Physical Review B*, 84(9):094302, 2011.

[40] Yoyo Hinuma, Giovanni Pizzi, Yu Kumagai, Fumiyasu Oba, and Isao Tanaka. Band structure diagram paths based on crystallography. *Computational Materials Science*, 128:140–184, 2017.

[41] Atsushi Togo, Laurent Chaput, Isao Tanaka, and Gilles Hug. First-principles phonon calculations of thermal expansion in Ti_3SiC_2, Ti_3AlC_2, and Ti_3GeC_2. *Physical Review B*, 81(17):174301, 2010.

[42] John P Perdew, Kieron Burke, and Matthias Ernzerhof. Generalized gradient approximation made simple. *Physical review letters*, 77(18):3865, 1996.

[43] John P Perdew, Adrienn Ruzsinszky, Gábor I Csonka, Oleg A Vydrov, Gustavo E Scuseria, Lucian A Constantin, Xiaolan Zhou, and Kieron Burke. Restoring the density-gradient expansion for exchange in solids and surfaces. *Physical review letters*, 100(13):136406, 2008.

[44] Aliaksandr V Krukau, Oleg A Vydrov, Artur F Izmaylov, and Gustavo E Scuseria. Influence of the exchange screening parameter on the performance of screened hybrid functionals. *The Journal of chemical physics*, 125(22):224106, 2006.

[45] Peter E Blöchl, Ove Jepsen, and Ole Krogh Andersen. Improved tetrahedron method for Brillouin-zone integrations. *Physical Review B*, 49(23):16223, 1994.

[46] Alex M Ganose, Keith T Butler, Aron Walsh, and David O Scanlon. Relativistic electronic structure and band alignment of BiSI and BiSeI: candidate photovoltaic materials. *Journal of Materials Chemistry A*, 4(6):2060–2068, 2016.

[47] Alex M Ganose, Madeleine Cuff, Keith T Butler, Aron Walsh, and David O Scanlon. Interplay of orbital and relativistic effects in bismuth oxyhalides: BiOF, BiOCl, BiOBr, and BiOI. *Chemistry of materials*, 28(7):1980–1984, 2016.

[48] Joachim Paier, Martijn Marsman, K Hummer, Georg Kresse, Iann C Gerber, and János G Ángyán. Screened hybrid density functionals applied to solids. *The Journal of chemical physics*, 124(15):154709, 2006.

[49] Soner Steiner, Sergii Khmelevskyi, Martijn Marsmann, and Georg Kresse. Calculation of the magnetic anisotropy with projected-augmented-wave methodology and the case study of disordered $Fe_{1-x}Co_x$ alloys. *Physical review B*, 93(22):224425, 2016.

[50] M Gajdoš, K Hummer, G Kresse, J Furthmüller, and FJPRB Bechstedt. Linear optical properties in the projector-augmented wave methodology. *Physical Review B*, 73(4):045112, 2006.

[51] Artem R Oganov, Chris J Pickard, Qiang Zhu, and Richard J Needs. Structure prediction drives materials discovery. *Nature Reviews Materials*, 4(5):331–348, 2019.

[52] Chris J Pickard and RJ Needs. Ab initio random structure searching. *Journal of Physics: Condensed Matter*, 23(5):053201, 2011.

[53] Artem R Oganov and Colin W Glass. Crystal structure prediction using ab initio evolutionary techniques: Principles and applications. *The Journal of chemical physics*, 124(24):244704, 2006.

[54] Yanchao Wang, Jian Lv, Li Zhu, and Yanming Ma. CALYPSO: A method for crystal structure prediction. *Computer Physics Communications*, 183(10):2063–2070, 2012.

[55] Junjie Wang, et al. MAGUS: machine learning and graph theory assisted universal structure searcher (under review).

[56] Kang Xia, Hao Gao, Cong Liu, Jianan Yuan, Jian Sun, Hui-Tian Wang, and Dingyu Xing. A novel superhard tungsten nitride predicted by machine-learning accelerated crystal structure search. *Science bulletin*, 63(13):817–824, 2018.

[57] Anubhav Jain, Shyue Ping Ong, Geoffroy Hautier, Wei Chen, William Davidson Richards, Stephen Dacek, Shreyas Cholia, Dan Gunter, David Skinner, Gerbrand Ceder, et al. Commentary: The Materials Project: A materials genome approach to accelerating materials innovation. *APL materials*, 1(1):011002, 2013.

[58] Harold T Stokes and Dorian M Hatch. FINDSYM: program for identifying the space-group symmetry of a crystal. *Journal of Applied Crystallography*, 38(1):237–238, 2005.

[59] Miquel Royo, Konstanze R Hahn, and Massimiliano Stengel. Using high multipolar orders to reconstruct the sound velocity in piezoelectrics from lattice dynamics. *Physical Review Letters*, 125(21):217602, 2020.

[60] Fredrik Eriksson, Erik Fransson, and Paul Erhart. The Hiphive Package for the extraction of high-order force constants by machine learning. *Advanced Theory and Simulations*, 2(5):1800184, 2019.

[61] Abel Carreras, Atsushi Togo, and Isao Tanaka. DynaPhoPy: A code for extracting phonon quasiparticles from molecular dynamics simulations. *Computer Physics Communications*, 221:221–234, 2017.